R. & M. No. 2966
(16,050)
(A.R.C. Technical Report)

MINISTRY OF SUPPLY

AERONAUTICAL RESEARCH COUNCIL
REPORTS AND MEMORANDA

Calculations of the Pressure Distributions and Boundary-layer Development on a Body of Revolution with Various Parabolic Afterbodies at Supersonic Speeds

By

L. E. FRAENKEL

LONDON: HER MAJESTY'S STATIONERY OFFICE
1957
PRICE 11s 6d NET

Calculations of the Pressure Distributions and Boundary-layer Development on a Body of Revolution with Various Parabolic Afterbodies at Supersonic Speeds

By

L. E. FRAENKEL

COMMUNICATED BY THE PRINCIPAL DIRECTOR OF SCIENTIFIC RESEARCH (AIR), MINISTRY OF SUPPLY

Reports and Memoranda No. 2966†

February, 1953

Summary.—Detailed calculations are made of the flow over a series of bodies at Mach numbers of 1·2, 1·4 and 1·6 and Reynolds numbers of 48 to 72 millions. The bodies consist of a basic forebody and parallel portion to which are added truncated parabolic afterbodies of three different thickness ratios. The calculations are in three main parts :

(i) Calculation of the inviscid flow over the bodies, mainly by the method of characteristics.

(ii) Calculation of the boundary-layer properties by what is essentially an extension to compressible flows of the method of Squire and Young.

(iii) Calculation of the pressure distribution on the ' modified ' afterbodies which result from adding the displacement thicknesses to the original profiles, by Ferri's method of linearized characteristics.

The results indicate that the slender body and quasi-cylinder theories predict the flow over afterbodies with only very limited accuracy for the thickness ratios and Mach numbers occurring in practice, but that the linearized similarity law remains a useful means of generalizing the particular results of exact inviscid-flow calculations. The boundary layers are seen to thicken very rapidly towards the rear of the afterbodies and this causes pressure changes of as much as 12 per cent of the peak suction. The skin-friction results agree extremely well with those for the equivalent flat plate.

1. *Introduction.*—This report is part of an experimental and theoretical investigation of afterbody drag and base drag. These two problems are intimately related, for analysis of the flow in the vicinity of the base, whether theoretical or experimental, can at most hope to formulate a law relating the base pressure to the pressure, flow direction, and boundary layer immediately ahead of the base[1]. Further, conditions in the neighbourhood of the base affect the pressures towards the rear of the afterbody by propagating disturbances upstream through the boundary layer : this effect is most serious at low Reynolds numbers.

In a first approach to the overall problem it seems reasonable to concentrate on moderate boat-tail angles and flows at high Reynolds numbers, so that a well-developed turbulent boundary layer approaches the base ; the effect of the flow behind the base on the afterbody pressures may then be expected to be small (in particular it is hoped that separation of the boundary layer ahead of the base will be avoided), and experimental evidence[1] also shows that for such flows the relation between the base pressure and the pressure ahead of the base is not particularly sensitive to changes of Reynolds number. It is also desirable initially to consider low supersonic Mach numbers in order to keep heat-transfer effects to a minimum. Fortunately it is this problem of flows with moderate boat-tail angles, at large Reynolds numbers and at low supersonic Mach numbers, which is also the most pressing from the viewpoint of the aircraft designer.

† R.A.E. Report Aero. 2482, received 1st September, 1953.

The present report is an attempt to calculate the pressure-distributions and boundary-layer properties on a related series of afterbodies subject to these conditions. It seems worthwhile to take considerable pains in performing such calculations because firstly they should provide more detailed and accurate information of afterbody drag than exists at the present time, and secondly they should indicate, when the accompanying experiments are made, whether more or less conventional methods of calculation can determine accurately the pressure and boundary layer immediately ahead of a base.

The calculations consist of three main parts :

(i) Calculation of the pressure distributions on the bodies in inviscid flow.

(ii) Calculation of the boundary-layer displacement thickness (and of other boundary-layer properties, in the process).

(iii) Calculation of the changes in the afterbody pressure distributions due to the addition of the displacement thicknesses to the body profiles.

These are of course only the initial steps of what should ideally be an iterative process ; however, it is doubtful whether further iterations are worthwhile in view of the approximate nature of the boundary-layer calculations, and in any case one would expect the results to converge fairly rapidly.

The bodies of revolution for which the calculations were made are shown in Fig. 1. They consist of a basic forebody and parallel portion to which are added three afterbodies of parabolic profile and various thickness ratios t (maximum radius/length of the afterbody continued to a point). A small cone angle and a long parallel portion were chosen in order to make the flow outside the boundary layers immediately ahead of the afterbodies virtually isentropic and uniform, afterbody effects being thus separated from the interference effects of the forebody. Nine such bodies are to be tested by the ground-launched technique ; they have the same basic shape as those in Fig. 1, but are truncated to have shorter afterbodies of various lengths. On the flight models the cone shoulder will also be rounded off to avoid local separation of the boundary layer.

Mach numbers of 1·2, 1·4 and 1·6 were taken in the calculations, and sea-level conditions were considered : Reynolds numbers, based on body length, were in the range of 48 to 72 millions. Zero incidence was assumed throughout.

2. *The method of Calculating the Pressure Distributions in Inviscid Flow.*—2.1. *Calculation of Pressures Due to the Conical Head.*—The velocity on the cone surface was taken from Ref. 2, and the pressure computed therefrom. Because of the small cone angle the inviscid flow is effectively isentropic throughout the field, the total pressure ratio across the cone shock being 1·00000 in all cases.

The pressures along the parallel portion were calculated by a modified form of the slender-body theory which is compared with exact theory in Fig. 2†. The ordinary slender-body theory[3] gives the following expression for the pressure on a parallel portion behind a conical head (this pressure coefficient is also the ' interference pressure coefficient ' of Ref. 4) :

$$C_p\left(\frac{l_F}{R}\right)^2 = 2\log\frac{x_1+1}{x_1} - \frac{2l_F}{\beta R}\,U\left(\frac{x_1 l_F}{\beta R}\right), \qquad (2.1.1)$$

where l_F is the length of the cone, R is its maximum radius, x_1 is $(x - l_F)/l_F$, β is $\sqrt{(M_0^2 - 1)}$,

† Tables of the pressure distribution on cone-cylinders[26] calculated by the method of characteristics have recently been published ; however, the use of these tables in the present case would have required not only a double interpolation and extrapolation (for cone angle and Mach number), but also an awkward numerical differentiation of the results, which would be available only at unequal intervals, in order to obtain the velocity gradients which are required for the boundary-layer problem.

The modified slender-body theory gives good agreement with the results of Ref. 26 (Fig. 2) and it was felt that the analytic formulae used would lead to greater overall consistency. The comparison of slender-body and exact theory made in Ref. 26 itself is wrong.

and U is a function tabulated in Refs. 4 and 5. The disadvantage of this formula is its logarithmic singularity at the cone shoulder ($x_1 = 0$), but this can easily be overcome by the following modification. Since the effect represented by the logarithmic term is by far the smaller one in (2.1.1) we replace it by a quadratic function in an initial interval of x_1 ($0 < x_1 \leqslant 0{\cdot}4$ was taken here) and choose the constants of this function to give C_p its exact value at the shoulder ($x_1 = 0$), and to fair it into the curve of (2.1.1), with continuity of slope, at the end of the interval ($x_1 = 0{\cdot}4$). The exact value of C_p at the shoulder can of course be calculated from Ref. 2 and Prandtl-Meyer expansion tables. The resulting expression is

$$C_p\left(\frac{l_F}{R}\right)^2 = b_0 + b_1 x_1 + b_2 x_1^2 - \frac{2l_F}{\beta R}\, U\left(\frac{x_1 l_F}{\beta R}\right), \quad 0 < x_1 \leqslant 0{\cdot}4\,, \qquad (2.1.2)$$

where
$$b_0 = C_p|_{x_1=0+} \cdot \left(\frac{l_F}{R}\right)^2 + \frac{2l_F}{\beta R}\,,$$
$$b_1 = 16{\cdot}099 - 5b_0,$$
$$b_2 = -24{\cdot}588 + 6{\cdot}250 b_0\,.$$

The other flow parameters required for the boundary-layer calculations (local Mach number, temperature, etc.) were computed from the pressure coefficient by means of the exact relationships for isentropic flow, which are tabulated in Ref. 6 and elsewhere. In particular, the relationship

$$C_p = \left\{\left(1 + \frac{\gamma - 1}{2} M^2\right)^{-\frac{\gamma}{\gamma - 1}} - \frac{p_0}{p_t}\right\} \frac{p_t}{\frac{1}{2}\rho_0 V_0^2}\,,$$

where $(\,)_t$ denotes total or stagnation and $(\,)_0$ denotes free-stream conditions, leads to the following expression for the velocity gradient :

$$\frac{1}{V}\frac{dV}{dx_1} = \frac{1}{M\left(1 + \frac{\gamma - 1}{2} M^2\right)} \frac{dM}{dx_1} = -\frac{1}{2}\frac{dC_p}{dx_1}\frac{M_0^2}{M^2}\frac{(p_0/p_t)}{(p/p_t)}\,.$$

Here dC_p/dx_1 may be calculated from (2.1.1), (2.1.2), (the derivative of the U-function is tabulated in Refs. 5 and 7), and the other quantities are tabulated functions of the free-stream and local Mach numbers.

γ was taken as $1{\cdot}400$ throughout the present calculations, the only inconsistency being that the values of velocity on the cone surface given in Ref. 2 were used, and these are based on $\gamma = 1{\cdot}405$ (this accounts for the discrepancy in the values of C_p at $x_1 = 0$ in Fig. 2).

2.2. *Calculation of Pressures on the Afterbodies.*—In the calculation of the afterbody flow fields it was assumed throughout that at the end of the parallel portion the disturbance from the cone had completely decayed, so that the flow immediately ahead of the afterbodies was uniform and at free-stream Mach number : in actual fact the Mach number varies, in the worst case, from $1{\cdot}604$ on the surface of the body to $1{\cdot}600$ at infinity.

The method of characteristics was used to calculate the flow fields : one of the characteristics networks is shown in Fig. 3. The particular form of equations used may be relevant.

The equations of the characteristic curves are of course

for C_1 $$\frac{dy}{dx} = \tan(\theta + \alpha)\,, \qquad (2.2.1)$$

and for C_2 $$\frac{dy}{dx} = \tan(\theta - \alpha)\,, \qquad (2.2.2)$$

where C_1 and C_2 denote characteristics of the first and second families, respectively, θ is the inclination of the velocity vector, and α is the Mach angle. The survey of Ref. 8 shows that for

wholly numerical calculations of high accuracy by far the most convenient form of the compatibility equations for axially symmetric, isentropic flow is that due to Guderley. This may be written

$$\text{for } C_1 \qquad \frac{dl}{dy} = \frac{90}{\pi}\frac{\sin\theta\sin\alpha}{\sin(\theta+\alpha)}\frac{1}{y}, \text{ where } l = \tfrac{1}{2}(\nu-\theta), \qquad (2.2.3)$$

$$\text{and for } C_2 \qquad \frac{dm}{dy} = \frac{90}{\pi}\frac{\sin\theta\sin\alpha}{\sin(\theta-\alpha)}\frac{1}{y}, \text{ where } m = \tfrac{1}{2}(\nu+\theta), \qquad (2.2.4)$$

ν being the Prandtl-Meyer angle. l, m, ν, θ are all in degrees, and l and m are of course curvilinear co-ordinates of the epicycloids in the hodograph plane of two-dimensional flows. The relationship between ν and α is carefully tabulated in Ref. 9.

The equations in this form are not only simpler than those in terms of the velocity V, but they also permit a sound 'initial guess' to be used in the step-by-step solution at points where the flow is nearly two-dimensional, for at such points one may write initially $dl \simeq 0$, $dm \simeq 0$.

In the present problem the equation of the afterbodies is most simply written

$$y_2 = t(1 - x_2^2), \qquad (2.2.5)$$

where

$$\frac{x_2}{x - l_F - l_p} = \frac{y_2}{y} = \frac{1}{l_A},$$

so that the boundary condition becomes

$$\theta = \tan^{-1}(-2tx_2),$$

on the body.

Some details of the numerical solution of these equations are given in Appendix I†.

3. *The Method of Calculating the Boundary-Layer Properties.*—3.1. *An Approximate Theory for Turbulent Boundary Layers in Axially Symmetric, Compressible Flow.*—The theory outlined below is essentially a simple extension to compressible flows of the method of Squire and Young[10, 11]; it should be noted, however, that in referring several parameters to conditions at the wall it differs from the extension tentatively suggested by Young himself in Ref. 12.

For the steady, axially symmetric flow of a compressible fluid the boundary-layer momentum equation may be written (*see*, for example, Ref. 12)

$$\frac{d\vartheta}{d\xi} + \left[\frac{1}{y}\frac{dy}{d\xi} + \frac{1}{\rho_1}\frac{d\rho_1}{d\xi} + \frac{H+2}{V_1}\frac{dV_1}{d\xi}\right]\vartheta = \frac{\tau_w}{\rho_1 V_1^2}, \qquad (3.1.1)$$

where

$$\vartheta = \text{momentum thickness} = \int_0^\delta \frac{\rho V}{\rho_1 V_1}\left(1 - \frac{V}{V_1}\right)\left(1 + \frac{\eta\cos\theta}{y}\right)d\eta,$$

$$\delta^* = \text{displacement thickness} = \int_0^\delta \left(1 - \frac{\rho V}{\rho_1 V_1}\right)\left(1 + \frac{\eta\cos\theta}{y}\right)d\eta,$$

$H = \delta^*/\vartheta$,

(ξ, η) are co-ordinates along and normal to the body profile,

$y(\xi)$ is the body radius,

† The numerical solution of these equations was done by the Computing Section of the Mathematics Division, National Physical Laboratory, under the supervision of Dr. L. Fox. One of the nine flow fields was also calculated at Royal Aircraft Establishment under the author's supervision; the 'deferred approach to the limit' (Appendix I) was not used, but the resulting values of α agreed with the N.P.L. results within $\frac{1}{3}$ per cent of the range in the field.

$\theta(\xi)$ is the inclination of the profile,

τ_w is the shear stress at the wall,

and $()_1$ denotes local conditions outside the boundary layer.

Now the equation of motion along a streamline gives

$$\frac{dp_1}{d\xi} = -\rho_1 V_1 \frac{dV_1}{d\xi} ,$$

so that $$\frac{1}{\rho_1}\frac{d\rho_1}{d\xi} = \frac{1}{\rho_1}\frac{d\rho_1}{dp_1}\frac{dp_1}{d\xi} = -\frac{1}{\rho_1}\frac{1}{a_1^2}\rho_1 V_1 \frac{dV_1}{d\xi} = -\frac{M_1^2}{V_1}\frac{dV_1}{d\xi} ;$$

and the energy equation gives

$$\frac{1}{V_1}\frac{dV_1}{d\xi} = \frac{1}{M_1\left(1 + \frac{\gamma - 1}{2} M_1^2\right)}\frac{dM_1}{d\xi} ,$$

so that (3.1.1) becomes

$$\frac{d\vartheta}{d\xi} + \left[\frac{1}{y}\frac{dy}{d\xi} + \frac{H + 2 - M_1^2}{M_1\left(1 + \frac{\gamma - 1}{2} M_1^2\right)}\frac{dM_1}{d\xi}\right]\vartheta = \frac{\tau_w}{\rho_1 V_1^2} . \quad .. \quad .. \quad (3.1.2)$$

In order to be able to solve this differential equation we must obtain expressions for H and τ_w in terms of known quantities and ϑ, and so we make the usual basic assumptions :

(A1) That the static pressure across the boundary layer is constant normal to the surface (this is already implicit in the momentum equation), and

(A2) That the effects of pressure gradient and of the axially symmetric nature of the flow on the boundary-layer *profile characteristics* can be neglected ; *i.e.*, that at any point on the body H and the relation between ϑ and τ_w are the same as for a flat plate with the same local conditions outside the boundary layer. Neglecting the effect of the axially symmetric nature of the flow on the profile characteristics is equivalent to treating as unity the factor $(1 + \eta \cos\theta/y)$ in the definitions of displacement and momentum thickness.

To solve the flat-plate problem we follow the approach of Cope[13] and Monaghan[14] and make the initial assumptions :

(A3) That the profile in the compressible turbulent boundary layer on a flat plate, with or without heat transfer, is given by

$$\frac{V}{V_{\tau w}} = \frac{1}{k}\log\frac{\eta V_{\tau w}}{a\nu_w} , \quad .. \quad .. \quad .. \quad .. \quad .. \quad .. \quad .. \quad .. \quad (3.1.3)$$

where $$V_{\tau w} = \sqrt{\left(\frac{\tau_w}{\rho_w}\right)} ,$$

$()_w$ denotes conditions at the wall, the constants k and a have the same values as in incompressible flow ($k = 0{\cdot}400$, $a = 0{\cdot}111$), and the logarithm is natural. Monaghan has provided some experimental justification for this assumption.

(A4) That Reynolds' analogy between momentum and heat exchange is valid, so that the temperature distribution in the boundary layer is given by

$$\frac{T}{T_w} = 1 - c_1 \frac{V}{V_1} - c_2 \frac{V^2}{V_1^2}, \qquad (3.1.4)$$

where $c_1 = 1 - \dfrac{T_{t1}}{T_w}$, and $c_2 = \dfrac{T_{t1}}{T_w} \cdot \dfrac{M_1^2}{M_1^2 + 2/(\gamma - 1)}$.

These assumptions lead to the approximate relations (*see* Appendix II) :

$$\frac{\vartheta V_1}{\nu_w} = C \exp\left(D \frac{V_1}{V_{\tau w}}\right), \qquad (3.1.5)$$

where $C = a/k$ and $D = k$,

and

$$\frac{H}{H_i} = \frac{T_w}{T_1} + \frac{\gamma - 1}{2} M_1^2, \qquad (3.1.6)$$

where H_i is the value given by the equivalent incompressible theory with the values V_1, ρ_1. The error in both these equations is given by a factor $[1 + O(V_{\tau w}/V_1)]$.

We now modify equations (3.1.5) and (3.1.6) in the light of experimental results.

(i) Because of the terms neglected in the derivation of (3.1.5) we evaluate C and D not from the known constants a and k but to give best agreement with the formula

$$C_{Fw} = 0{\cdot}455 \left(\log_{10} R_{ew} \frac{T_1}{T_w}\right)^{-2{\cdot}58}, \qquad (3.1.7)$$

which is the extension of Prandtl's well-known formula in incompressible flow and for which Monaghan has also given experimental justification. Now it may be shown (Appendix II) that the same constants C and D which give the best agreement between

$$\frac{\vartheta V_1}{\nu} = C \exp\left(D \frac{V_1}{V_\tau}\right) \quad \text{and} \quad C_F = 0{\cdot}455\,(\log_{10} R_e)^{-2{\cdot}58}$$

in the incompressible case, also give the best agreement between (3.1.5) and (3.1.7) in the compressible case, and so we may take Squire and Young's values $C = 0{\cdot}2454$ and $D = 0{\cdot}3914$.

(ii) Reynolds' analogy gives for zero heat transfer at the wall $T_w = T_{t1}$, i.e.,

$$\frac{T_w}{T_1} = 1 + \frac{\gamma - 1}{2} M_1^2.$$

Better agreement with experiment for this case is given by Squire's formula

$$\frac{T_w}{T_1} = 1 + \frac{\gamma - 1}{2} \sigma^{1/3} M_1^2, \qquad (3.1.8)$$

where σ is the Prandtl number. This suggests rewriting (3.1.6) as

$$\frac{H}{H_i} = \frac{T_w}{T_1} + \frac{\gamma - 1}{2} \sigma^{1/3} M_1^2, \qquad (3.1.9)$$

which also gives better agreement with experiment than (3.1.6).

We now make our final assumption :

(A5) That there is zero heat transfer at the wall.

We may then use (3.1.8) throughout, and we have for substitution into (3.1.2)

$$\frac{H}{H_i} = 1 + (\gamma - 1)\,\sigma^{1/3} M_1^{\,2}\,, \qquad \text{(3.1.10)}$$

and

$$\frac{V_{\tau w}^{\,2}}{V_1^{\,2}} = \frac{\tau_w}{\rho_w V_1^{\,2}} = \frac{D^2}{\log^2\left(\dfrac{\vartheta V_1}{C\nu_w}\right)}\,. \qquad \text{(3.1.11)}$$

Thus (3.1.2) becomes

$$\frac{d\vartheta}{d\xi} + \left\{ \frac{1}{y}\frac{dy}{d\xi} + \frac{H_i + 2 + [H_i(\gamma-1)\sigma^{1/3} - 1]M_1^{\,2}}{M_1\left(1 + \dfrac{\gamma-1}{2} M_1^{\,2}\right)} \frac{dM_1}{d\xi} \right\} \vartheta$$

$$= \frac{T_1}{T_w} \frac{D^2}{\log^2\left(\dfrac{\vartheta V_1}{C\nu_w}\right)}\,, \qquad \text{(3.1.12)}$$

where T_1/T_w is given by (3.1.8). If the external flow field is known this differential equation can be integrated numerically, step by step†.

3.2. *Application of the Approximate Theory to the Present Problem.*—3.2.1. *Values of the constants.*—The following constants were used in the approximate theory above.

$$\begin{aligned} H_i &= 1{\cdot}400 \\ \gamma &= 1{\cdot}400 \\ \sigma &= 0{\cdot}715 \qquad \sigma^{1/2} = 0{\cdot}8456 \qquad \sigma^{1/3} = 0{\cdot}8942 \\ C &= 0{\cdot}2454 \qquad D = 0{\cdot}3914. \end{aligned}$$

---

† After this work had been completed Professor A. D. Young pointed out that in problems of axially symmetric flow it is important to work with the displacement and momentum areas,

$$A_{\delta^*} = 2\pi y \delta^* \quad \text{and} \quad A_\vartheta = 2\pi y \vartheta\,.$$

Thus equation (3.1.12) may be written

$$\frac{dA_\vartheta}{d\xi} + \frac{H_i + 2 + [H_i(\gamma-1)\sigma^{1/3} - 1]M_1^{\,2}}{M_1\left(1 + \dfrac{\gamma-1}{2} M_1^{\,2}\right)} \frac{dM_1}{d\xi} A_\vartheta$$

$$= 2\pi y \frac{T_1}{T_w} \frac{D^2}{\log^2\left(\dfrac{A_\vartheta V_1}{2\pi y C\nu_w}\right)}\,,$$

and, unlike ϑ, A_ϑ remains bounded as $y \to 0$.

Further, it is not the displacement thickness δ^* which should be added to the body profiles, but the 'effective displacement thickness' δ_1^*, which corresponds *exactly* to the displacement area and is therefore defined by

$$A_{\delta^*} = \pi \sec\theta\,[(y + \delta_1^* \cos\theta)^2 - y^2]$$

or

$$\delta_1^* = \sec\theta\,[-y + \sqrt{(y^2 + 2y\delta^* \cos\theta)}]\,.$$

δ^* and δ_1^* are equal to first order in (δ^*/y), so that one might expect that the error of adding δ^* instead of δ_1^* to the profiles would not have too great an effect in the present work. Estimates have in fact indicated that this effect is of the same order of magnitude as the error introduced by the use of linearized characteristics but of opposite sign.

Viscosity was evaluated from Sutherland's formula, which, using the values given in Ref. 15, may be written

$$\mu = 3{\cdot}0997.\frac{T^{3/2}}{T + 117} \cdot 10^{-8} \text{ slugs/ft-sec},$$

where the temperature T is in degrees Kelvin.

3.2.2. *The boundary layer on the cone and the transition point.*—To start the boundary-layer calculations the following assumptions were made :

(i) That the transition point occurred at the cone shoulder.

(ii) That the momentum thickness was continuous through the transition point.

These assumptions were made because of the difficulty of predicting the transition point accurately, because the initial boundary layer was expected to have only a small effect on that over the afterbodies, and for the sake of convenience ; they may, however, be unnecessarily crude.

To calculate the laminar boundary layer on the cone the result[16] was used that for a flat plate and a cone with the same external flow

$$\vartheta(\text{cone}) = \frac{1}{\sqrt{3}}\vartheta \text{ (flat plate)}.$$

This relation again treats as unity the factor $(1 + \eta \cos\theta/y)$ in the definition of the momentum thickness on a body of revolution. For calculation of the laminar boundary layer on the equivalent flat plate the analysis of Ref. 17 was used.

3.2.3. *The practical form of the differential equation for* ϑ.—The differential equation (3.1.12) forms the basis of calculation of the turbulent boundary layer on the parallel portion and afterbodies, but its solution is more convenient if the variables x_1 and x_2 are introduced in place of ξ. We have for the parallel portion

$$\frac{d\xi}{dx_1} = \frac{dx}{dx_1} = l_F,$$

and for the afterbodies

$$\frac{d\xi}{dx_2} = \frac{d\xi}{dx}\frac{dx}{dx_2} = \sqrt{(1 + 4t^2x_2^2)}\,l_A,$$

$$\frac{1}{y}\frac{dy}{d\xi} = -\frac{2x_2}{1 - x_2^2}\frac{dx_2}{d\xi}.$$

Hence (3.1.12) may be written

$$\frac{d\vartheta}{dX} = \frac{g(X)}{\log^2[\vartheta(X)\,j(X)]} - h(X)\vartheta(X), \qquad (3.2.1)$$

where for the parallel portion

$$X = x_1$$

$$g(x_1) = l_F\frac{T_1}{T_w}D^2$$

$$j(x_1) = V_1C/\nu_w$$

$$h(x_1) = \frac{H_i + 2 + [H_i(\gamma - 1)\sigma^{1/3} - 1]M_1^2}{M_1\left(1 + \dfrac{\gamma - 1}{2}M_1^2\right)}\frac{dM_1}{dx_1} = \frac{3{\cdot}4000 - 0{\cdot}4992M_1^2}{M_1(1 + 0{\cdot}2M_1^2)}\frac{dM_1}{dx_1},$$

and for the afterbodies

$$X = x_2$$

$$g(x_2) = l_A\sqrt{(1 + 4t^2\, x_2{}^2)}\,\frac{T_1}{T_w}\,D^2$$

$$j(x_2) = V_1 C/\nu_w$$

$$h(x_2) = -\frac{2x_2}{1 - x_2{}^2} + \frac{3\cdot 4000 - 0\cdot 4992 M_1{}^2}{M_1(1 + 0\cdot 2M_1{}^2)}\frac{dM_1}{dx_2}\,.$$

The functions g, j, and h of course depend only on the external flow and on the equation for the wall temperature (3.1.8). Details of the numerical integration are given in Appendix I.

3.2.4. *Skin friction.*—Equation (3.1.11) gives the local skin-friction coefficient as

$$C_f = \frac{\tau_w}{\frac{1}{2}\rho_1 V_1{}^2} = 2\,\frac{T_1}{T_w}\,\frac{D^2}{\log^2\left(\dfrac{\vartheta V_1}{C\nu_w}\right)}\,.$$

For the parallel portion this may be written

$$C_f = \frac{2}{l_F}\,\frac{g(x_1)}{\log^2\left[\vartheta(x_1)\, j(x_1)\right]}\,,$$

and for the afterbodies

$$C_f = \frac{2}{l_A\sqrt{(1 + 4t^2 x_2{}^2)}}\,\frac{g(x_2)}{\log^2\left[\vartheta(x_2)\, j(x_2)\right]}\,.$$

Thus C_f follows immediately from integration of the differential equation.

The total skin-friction coefficient for the parallel portion is given by

$$C_F = \frac{1}{A_1}\int_0^{2\cdot 0}\frac{2g(x_1)}{\log^2[\vartheta(x_1)\, j(x_1)]}\,\frac{\rho_1 V_1{}^2}{\rho_0 V_0{}^2}\,2\pi R\, dx_1\,, \qquad (3.2.2)$$

and that for the parallel portion and an afterbody together by

$$C_F = \frac{1}{A_1 + A_2}\left\{\int_0^{2\cdot 0}\frac{2g(x_1)}{\log^2[\vartheta(x_1)\, j(x_1)]}\,\frac{\rho_1 V_1{}^2}{\rho_0 V_0{}^2}\,2\pi R\, dx_1 + \int_0^{0\cdot 648}\frac{2g(x_2)}{\log^2[\vartheta(x_2)\, j(x_2)]}\,\frac{\rho_1 V_1{}^2}{\rho_0 V_0{}^2}\,2\pi R(1 - x_2{}^2)\, dx_2\right\} \qquad (3.2.3)$$

where A_1 and A_2 are the wetted areas of the parallel portion and afterbody, respectively, so that

$$A_1 = 32\pi R^2\,,$$

and

$$A_2 = \int_0^{0\cdot 648} 2\pi R(1 - x_2{}^2)\,\sqrt{(1 + 4t^2 x_2{}^2)}\, l_A\, dx_2$$

$$= 2\pi t\, l_A{}^2\left[\left(1 + \frac{1}{16t^2}\right)\left(\frac{x_2}{2}\sqrt{(1 + 4t^2 x_2{}^2)} + \frac{1}{4t}\sinh^{-1} 2tx_2\right) - \frac{x_2}{16t_2}\,(1 + 4t^2 x_2{}^2)^{3/2}\right]\Bigg|_{x_2 = 0\cdot 648}$$

4. *The Method of Calculating Pressure Distributions on the Modified Afterbodies.*—4.1. *The Geometry of the Modified Afterbodies.*—Integration of the differential equation (3.2.1) left us with values of ϑ and $d\vartheta/dx_2$ at the integration stations. The modified afterbodies were then defined by

$$y = R(1 - x_2^2) + \delta^* \sqrt{(1 + 4t^2 x_2^2)} \,, \qquad \ldots \quad (4.1.1)$$

where $\delta^* = H_i[1 + (\gamma - 1)\sigma^{1/3} M_1^2]\vartheta \,,$

and their slope was given by

$$\frac{dy}{dx} = \frac{1}{l_A}\left[- 2Rx_2 + \frac{4t^2 x_2}{\sqrt{(1 + 4t^2 x_2^2)}}\,\delta^* + \sqrt{(1 + 4t^2 x_2^2)}\,\frac{d\delta^*}{dx_2}\right],$$

where

$$\frac{d\delta^*}{dx_2} = \frac{d\vartheta}{dx_2} H_i[1 + (\gamma - 1)\sigma^{1/3} M_1^2] + 2\vartheta H_i(\gamma - 1)\sigma^{1/3} M_1 \frac{dM_1}{dx_2} \,. \qquad \ldots \quad (4.1.2)$$

For the work of the following section the co-ordinates of the modified afterbodies were multiplied by $t/[R + \delta^*|_{x_2 = 0}]$, in order that their boundaries should start at the same points as those of the original bodies in the characteristics diagrams (Fig. 3). Thus variables x_3, y_3 were introduced, comparable to x_2, y_2, such that

$$\frac{x_3}{x - l_F - l_p} = \frac{y_3}{y} = \frac{1}{l_A[1 + (\delta^*|_{x_3 = 0}/R)]} = \frac{1}{l_A(1 + \varepsilon)} \,,$$

and the equations of the modified bodies in the characteristics diagrams became

$$y_3 = \frac{1}{1 + \varepsilon}\left\{ t[1 - x_3^2(1 + \varepsilon)^2] + \sqrt{\{1 + 4t^2 x_3^2 (1 + \varepsilon)^2\}}\,\frac{\delta^*}{l_A}\right\} \,. \qquad \ldots \quad (4.1.3)$$

For the presentation of results, however, the modified bodies were scaled up again by the factor $(1 + \varepsilon)$, and account was taken of the fact that the pressure had been assumed constant in the boundary layer along lines normal to the body surface, and not along lines $x_2 =$ constant.

4.2. *The Method of Linearized Characteristics.*—To calculate the change in the pressure distributions on the afterbodies due to the presence of the boundary layers Ferri's method of linearized characteristics[18] was used. The essential basis of this method is as follows.

Consider perturbations superposed upon a known flow field such that the original velocities $(u_0, v_0, 0)$ are changed to $(u_0 + u_1, v_0 + v_1, w_1)$, where (u_1, v_1, w_1) are small. By writing down the exact differential equation of supersonic flow first in terms of $(u_0 + u_1, v_0 + v_1, w_1)$ and then in terms of $(u_0, v_0, 0)$, subtracting the two equations, and neglecting terms of higher order than the first in (u_1, v_1, w_1), Ferri obtained a differential equation for (u_1, v_1, w_1) whose characteristic curves are those of the original flow field, that is

$$\frac{dy}{dx} = \tan(\theta_0 \pm \alpha_0) \,. \qquad \ldots \quad (4.2.1)$$

(It is important that the characteristic curves of the differential equation for the complete new flow $(u_0 + u_1, v_0 + v_1, w_1)$ are not those of the original field.) Ferri went on to develop the compatibility equations of the perturbation field; however, he worked with variables which were not considered to be the most convenient for the present problem. His compatibility equations for isentropic axially symmetric flow have therefore been transformed into the following form (Appendix III):

for C_1 $$\frac{d\alpha_1}{dy} + D_1 \frac{d\theta_1}{dy} - (D_1 F_1 + E_1)\theta_1 - \left(G_1 \frac{d\alpha_0}{dy} + E_1\right)\alpha_1 = 0 \,, \qquad \ldots \quad (4.2.2)$$

and for C_2

$$\frac{d\alpha_1}{dy} - D_2\frac{d\theta_1}{dy} + (D_2F_2 + E_2)\theta_1 - \left(G_2\frac{d\alpha_0}{dy} + E_2\right)\alpha_1 = 0, \qquad .. \quad (4.2.3)$$

where

$$D_1 = D_2 = \frac{2\sin^2\alpha_0 + \gamma - 1}{2\cos^2\alpha_0}$$

$$E_1 = \left(\frac{d\alpha_0}{dy}\right)_{(2)}\frac{2\sin(\theta_0 - \alpha_0)}{\sin 2\alpha_0 \sin(\theta_0 + \alpha_0)} \qquad E_2 = \left(\frac{d\alpha_0}{dy}\right)_{(1)}\frac{2\sin(\theta_0 + \alpha_0)}{\sin 2\alpha_0 \sin(\theta_0 - \alpha_0)}$$

$$F_1 = \frac{\sin(\theta_0 - \alpha_0)}{\sin(\theta_0 + \alpha_0)}\frac{1}{y} \qquad F_2 = \frac{\sin(\theta_0 + \alpha_0)}{\sin(\theta_0 - \alpha_0)}\frac{1}{y}$$

$$G_1 = G_2 = \tan\alpha_0\frac{2(\gamma + 1)}{2\sin^2\alpha_0 + (\gamma - 1)}.$$

$(d\alpha_0/dy)_{(1)}$ and $(d\alpha_0/dy)_{(2)}$ are total derivatives along the first and second family characteristics, respectively. Because the coefficients are all known no iteration is required in the solution of these equations. A convenient form of procedure for solving the equations is given in Appendix III.

Calculations by the method of linearized characteristics were made in the present work only for the four cases $t = 0{\cdot}1$, $M_0 = 1{\cdot}2$, $1{\cdot}6$ and $t = 0{\cdot}2$, $M_0 = 1{\cdot}2$, $1{\cdot}6$. For the other five cases the results in the form $\Delta C_p/|C_{p\,\min}|$ were interpolated linearly with respect to M_0 and t, for $x_2 > 0$. The systematic variation both of the changes in the boundary condition and of the results for $\Delta C_p/|C_{p\,\min}|$ (*see* Fig. 5) suggested that very little accuracy was lost by this interpolation. The two-dimensional pressure jumps at $x_2 = 0$, which are discussed in section 5.2, were calculated exactly for all nine cases.

5. *Results.*—5.1. *General.*—The principal results of the calculations are presented in Tables 1 to 4. The results for inviscid flow, with the exception of the parameter $dV_1/V_1\,dx$ for the afterbodies, are considered to be accurate in general to the number of places shown, but they are of course subject to the assumptions of the theory used. In the results depending on the boundary-layer calculations, and in the values of $dV_1/V_1\,dx$ for the afterbodies, the last figure has probably little or no absolute significance, even within the assumptions of the theory ; it has been included because in certain cases it is believed to be significant in indicating the change in a parameter between adjacent points (*e.g.*, in the values of δ^* over the initial part of the afterbodies).

Where they illustrate points of interest, the results have also been presented as graphs : these figures are mainly self-explanatory, but certain features of them are discussed below.

5.2. *Pressure Distributions and Wave Drag Coefficients.*—The complete pressure distributions on the bodies in inviscid flow are shown in Fig. 4. The changes in afterbody pressure due to the presence of boundary layers are shown in Fig. 5, and the afterbody pressure distributions, with and without this effect, are shown in Fig. 6. It is apparent that the boundary layers can cause pressure changes of the order of 12 per cent of the peak suction. The changes in pressure at the beginning of the afterbodies are two-dimensional pressure jumps, resulting from the slope of the modified afterbodies at $x_2 = 0 +$; in practice these discontinuities would of course be rounded off, but some remnant of the pressure change might still appear, distributed over a finite interval.

Results obtained by exact characteristics theory are compared with those of the linearized characteristics method in Fig. 6c for the case $t = 0{\cdot}2$, $M_0 = 1{\cdot}6$, which was expected to be the worst case from this viewpoint†.

† The exact characteristics calculations were done by Mathematical Services Department, R.A.E., under the supervision of P. Birchall. The technique was that outlined in section 2.2 and Appendix I.

In Fig. 7 the pressure and drag coefficients predicted by the slender-body[3,5] and quasi-cylinder[5,7] solutions of the linearized equation are compared with the results of the present calculations for inviscid flow. The two cases shown are the best and worst from the viewpoint of linearized theory : it is apparent that for a given value of βt the slender body theory is rather less accurate for afterbodies than it is for forebodies and that the quasi-cylinder theory fails to predict recompression towards the rear of the bodies. The apparent discrepancy in Fig. 7a, where the quasi-cylinder theory underestimates the magnitude of the pressure coefficient but overestimates the drag coefficient over the initial part of the afterbody, is due to the approximate expression which this theory uses for the derivative of the cross-sectional area. The slender body formulae are[4] :

$$C_p = 4t^2 \left[(3x_2^2 - 1) \log \frac{2x_2}{\beta t(1 - x_2^2)} - \frac{11}{2} x_2^2 \right],$$

and

$$C_D = 4t^2 l_2^2 \left[2(1 - l_2^2) \log \frac{2l_2}{\beta t(1 - l_2^2)} - \frac{10}{3} l_2^4 + \frac{11}{2} l_2^2 - 1 \right],$$

where l_2 is the ratio of the truncated body length to pointed body length.

In the quasi-cylinder theory the choice of mean radius is always arbitrary : for the pressure distributions of Fig. 7 arithmetic means of the radii at $x_2 = 0$ and $x_2 = 0{\cdot}648$ were used, but for the drag coefficients arithmetic means of the radii at $x_2 = 0$ and $x_2 = l_2$ were used. The resulting formulae are[4] :

$$C_p = -2t^2 (2 - l_2^2) U_1 \left[\frac{2x_2}{\beta t(2 - l_2^2)} \right], \quad l_2 = 0{\cdot}648,$$

and

$$C_D = t^2 \cdot \frac{\beta^2 t^2}{2} (2 - l_2^2)^4 T \left[\frac{2l_2}{\beta t(2 - l_2^2)} \right],$$

where U_1 and T are functions tabulated in Ref. 4.

While the accuracy of these theories leaves something to be desired where practical applications are concerned, the supersonic similarity law, which is also based on the linearized equation, provides a useful means of generalizing results for quite large values of βt and for all x_2 and l_2. This law states that for geometrically similar bodies C_p/t^2 and C_D/t^2 are functions of x_2 (or l_2) and βt only† ; it is particularly useful because for moderately slender bodies at high Mach numbers it goes over into the hypersonic similarity law[19, 20, 21].

The extent to which the law holds is illustrated by Figs. 8 and 9 ; the results shown are of course those for inviscid flow. It may be noted that although the results for different bodies do not ' collapse ' completely into a single curve, the error of the law is systematic and nearly always in the same direction ; that is, if the curve for some particular thickness ratio (or some particular Mach number) is assumed to be unique, it will always overestimate the drag for larger thickness ratios (or lower Mach numbers), and underestimate the drag for smaller thickness ratios (or higher Mach numbers). This trend also appears in other applications of the similarity law[22]. Thus if it should be required to use the law to obtain results of really high accuracy, this could be done by plotting known results for t = constant (or M_0 = constant) according to the law, and by then applying a small correction when this data is applied to unknown flows. This correction would be of the form

$$\frac{\partial}{\partial t}\left(\frac{C_D}{t^2}\right)\Bigg|_{\substack{\beta t = \text{constant} \\ l_2 = \text{constant}}} \cdot \Delta t \quad \text{or} \quad \frac{\partial}{\partial M_0}\left(\frac{C_D}{t^2}\right)\Bigg|_{\substack{\beta t = \text{constant} \\ l_2 = \text{constant}}} \cdot \Delta M,$$

and the value of the partial derivatives could be estimated from such results as those of Fig. 9.

† Clearly an alternative form is that $C_D l_2^2/t^2$ is a function of l_2 and $\beta t/l_2$ only : this is the form that has been used in Fig. 9.

The present results for the pressures and drags on parabolic afterbodies have been generalized by means of the similarity law and presented in a form suitable for design use in Ref. 22.

5.3. *The Boundary Layers.*—Fig. 10 shows the growth of the boundary-layer momentum and displacement thicknesses along the bodies ; the effect of Mach number is illustrated in Fig. 11.

Over the rear half of the parallel portion, where the pressure gradient is negligible, a good approximation to the boundary-layer growth is given by

$$\vartheta = K . R_{ex}^{-1/5} . x$$

where x is measured from the effective starting point of the turbulent boundary layer (obtained by extrapolation to $\vartheta = 0$) and R_{ex} is based on free-stream Mach number. Values of K obtained from the present results are compared with those predicted by the 1/7 power law for the velocity profile on a flat plate[13,14] in the following table.

M_0	K (from present results)	K (flat plate)
1·2	0·0375	0·0328
1·4	0·0354	0·0318
1·6	0·0335	0·0307

The increased values of K here are of course due to the initial adverse pressure gradient.

The rapid thickening of the boundary layer towards the rear of the afterbodies is due principally to the axially symmetric nature of the flow : since mass is conserved between adjacent stream surfaces, these surfaces must diverge appreciably when the radius of the body becomes sufficiently small. In the boundary-layer momentum equation this effect is realized by the term $dy/y\, d\xi$, which becomes the dominant one.

The marked growth of the boundary-layer displacement thickness is of course responsible for the appreciable pressure changes encountered above.

Total skin-friction coefficients are presented in Table 4 : the corresponding values of flat-plate skin friction, as predicted by Cope's log law[13], are also given for the sake of comparison. The effect of pressure gradients is seen to be negligible, but it must be remembered that the boundary layers on the bodies were assumed to have flat-plate profiles of the type used in Cope's theory.

6. *Conclusions.*—The emphasis in this work has been on the presentation of quantitative data in a systematic form, suitable for comparison with experiment ; consequently there is little of a new or startling nature in the conclusions below. They are, however, felt to be fairly generally valid for the afterbody problem.

(i) The slender body and quasi-cylinder solutions of the linearized equation do not predict the inviscid flow over afterbodies as accurately as they do the flow over forebodies and parallel portions ; the slender body theory gives good accuracy only for extremely small values of the parameter βt (for $\beta t > 0{\cdot}07$ the error is more than 10 per cent), and the quasi-cylinder theory fails to predict recompression towards the rear of the bodies.

(ii) The supersonic similarity law, which is also based on the linearized equation, is a useful tool for generalizing particular inviscid flow results ; if the pressure and drag coefficients on bodies with maximum slopes up to 0·4 are plotted according to the law, the maximum deviation from a mean curve is about 5 per cent, and this error is nearly always a systematic one for which allowance could be made.

(iii) As at subsonic speeds the boundary layer towards the rear of an afterbody thickens extremely rapidly. On the modified afterbody which results from adding the displacement thickness to the body profile, suctions were reduced by as much as 12 per cent of the maximum in the present calculations, and towards the rear of the body this effect is increasing rapidly.

(iv) The effect of pressure gradients and of axially symmetric flow on the total skin-friction drag of a turbulent boundary layer appears to be negligible.

LIST OF SYMBOLS

(Symbols which appear only once in the text and are defined there are not included in this list.)

a	Constant in the equation of the turbulent boundary-layer profile (3.1.3) and (II.1)
C	Constant used by Squire and Young, equation (3.1.5)
C_1	Characteristic curve of the first family
C_2	Characteristic curve of the second family
C_D	Wave drag coefficient based on maximum cross-section area
C_F	Total skin-friction coefficient, based on $\frac{1}{2}\rho_0 V_0^2$
C_f	Local skin-friction coefficient, $\tau_w/\frac{1}{2}\rho_1 V_1^2$
C_p	Pressure coefficient $(p - p_0)/\frac{1}{2}\rho_0 V_0^2$
c_1	$1 - T_{t1}/T_w$
c_2	$T_{t1}M_1^2/T_w[M_1^2 + 2/(\gamma - 1)]$
D	Constant used by Squire and Young, equation (3.1.5)
D_1, D_2 E_1, E_2 F_1, F_2 G_1, G_2	Coefficients in the compatibility equations of the linearized characteristics, equations (4.2.2), (4.2.3) or (III.8), (III.9)
g	Function appearing in the boundary-layer momentum equation (3.2.1)
H	δ^*/ϑ
h	Function appearing in the boundary-layer momentum equation (3.2.1)
j	Function appearing in the boundary-layer momentum equation (3.2.1)
k	Constant in the equation of the turbulent boundary-layer profile (3.1.3) and (II.1)
l_2	Length of truncated afterbody/length of afterbody continued to a point
l_A	Length of afterbody continued to a point
l_F	Length of forebody
l_p	Length of parallel portion
M	Mach number
p	Static pressure

LIST OF SYMBOLS—*continued*

R		Maximum radius of body
R_e		Reynolds number based on body or plate length
S		Cross-section area
t		Thickness ratio R/l_A
V		Velocity (inside the boundary layer in section 3.2 and Appendix II)
$V_{\tau w}$	=	$\sqrt{(\tau_w/\rho_w)}$
x		Axial co-ordinate (inches) measured from the nose
x_1	=	$(x - l_F)/l_F$
x_2	=	$(x - l_F - l_p)/l_A$
x_3		*See* equation (4.1.3)
y		Radial co-ordinate (inches)
y_2	=	y/l_A
y_3		*See* equation (4.1.3)
α		Mach angle
β	=	$\sqrt{(M_0^2 - 1)}$
γ		Ratio of the specific heats of air
δ		Boundary-layer thickness
δ^*		Boundary-layer displacement thickness
ζ	=	$V_1/V_{\tau w}$
η		Co-ordinate normal to the body surface
θ		Angle between the velocity vector and the x-axis
ϑ		Boundary-layer momentum thickness
ν		Kinematic viscosity
ξ		Co-ordinate along the body surface
ρ		Density
σ		Prandtl number
τ		Shear stress
$( )_0$		Conditions in the free stream *or*, in the linearized characteristics method, conditions in the original flow field
$( )_1$		Conditions outside the boundary layer *or*, in the linearized characteristics method, perturbations in the flow field
$( )_i$		Conditions in an equivalent incompressible problem
$( )_t$		Total or stagnation conditions
$( )_w$		Conditions referred to the density, viscosity, or temperature at the wall

REFERENCES

No.	*Author*	*Title, etc.*
1	D. R. Chapman	An analysis of base pressure at supersonic velocities and comparison with experiment. N.A.C.A. Tech. Note 2137. July, 1950.
2	Z. Kopal	Supersonic flow of air around cones. Massachusetts Institute of Technology Report No. 1. 1947.
3	M. J. Lighthill	Supersonic flow past slender bodies of revolution the slope of whose meridian section is discontinuous. *Quart. J. Mech. App. Maths*, Vol. 1, Pt. 1. March 1948.
4	L. E. Fraenkel	The theoretical wave drag of some bodies of revolution. R. & M. 2842. May, 1951.
5	M. J. Lighthill	Supersonic flow past bodies of revolution. R. & M. 2003. January 1945.
6	D. E. Lindop, E. E. Regan and R. Harrop	Tables for compressible air flow calculations, Part III. R.A.E. Tech. Note Aero. 1738b. A.R.C. 11,118. March, 1947.
7	G. N. Ward	The approximate external and internal flow past a quasi-cylindrical tube moving at supersonic speeds. *Quart. J. Mech. App. Maths*, Vol. 1, Pt. 2. June, 1948.
8	J. S. Isenberg	The method of characteristics in compressible flow, Part I. H.Q. Air Mat. Comm., Wright Field, Tech. Report F–TR–1173A–ND. 1947.
9	P. S. Herbert and S. J. Older	Tables for use in the investigation of supersonic fields of flow by the method of characteristics. R.A.E. Tech. Note CW1. A.R.C. 10,261. November, 1946.
10	H. B. Squire and A. D. Young	The calculation of the profile drag of aerofoils. R. & M. 1838. November, 1937.
11	A. D. Young	The calculation of the total and skin friction drags of bodies of revolution at zero incidence. R. & M. 1874. April, 1939.
12	A. D. Young	*Modern developments in fluid dynamics*, Vol. III, Chap. X ; Boundary layers. A.R.C. 12,472. July, 1949.
13	W. F. Cope	Notes and graphs for boundary-layer calculations in compressible flow. C.P. 89. August, 1951.
14	R. J. Monaghan and J. E. Johnson	The measurement of heat transfer and skin friction at supersonic speeds. Part II : Boundary-layer measurements on a flat plate at $M = 2{\cdot}5$ and zero heat transfer. C.P. 64. December, 1949.
15	G. W. C. Kaye and T. H. Laby	*Tables of physical and chemical constants*. Tenth edition. Longmans, Green and Co., London. 1948.
16	W. Hantzche and H. Wendt	The laminar boundary layer on a circular cone at zero incidence in a supersonic stream. Ministry of Supply (A) Völkenrode Report and Translation 276. 1946.
17	R. J. Monaghan	An approximate solution of the compressible laminar boundary layer on flat plate. R. & M. 2760. November, 1949.
18	A. Ferri	The linearized characteristics method and its application to practical non-linear supersonic problems. N.A.C.A. Tech. Note 2515. October, 1951.
19	H. S. Tsien	Similarity laws of hypersonic flows. *Jour. Maths. Phys.*, Vol. 25, No. 3. October, 1946.
20	W. D. Hayes	On hypersonic similitude. *Quart. App. Maths.*, Vol. 5. No. 1. April, 1947.
21	M. D. Van Dyke	The combined supersonic-hypersonic similarity rule. *J. Ae. Sci.*, Vol. 18, No. 7. July, 1951.

REFERENCES—*continued*

No.	*Author*	*Title, etc.*
22	L. E. Fraenkel	Curves for estimating the wave drag of some bodies of revolution, based on exact and approximate theories. C.P. 136. August, 1952.
23	W. J. Bickley	Formulae for numerical differentiation. *Mathematical Gazette*, Vol. XXV, No. 263. February, 1941.
24	W. J. Bickley	Formulae for numerical integration. *Mathematical Gazette*, Vol. XXIII, No. 256. October, 1939.
25	—	Interpolation and allied tables. H.M. Stationery Office, London. 1936.
26	R. F. Clippinger, J. H. Giese and W. C. Carter	Tables of supersonic flows about cone cylinders. Part I : Surface data. Ball Res. Labs., Aberdeen, BRL Report 729 (P.30972). 1950.

APPENDIX I

Some Details of Various Numerical Problems

I.1. *Application of the Exact Method of Characteristics.*—The differential equations (2.2.1) to (2.2.4) were replaced by difference equations, of the form

for C_1 $$\frac{\Delta y}{\Delta x} = \tan(\bar{\theta} + \bar{\alpha})$$

$$\frac{\Delta l}{\Delta y} = \frac{90}{\pi} \frac{\sin\bar{\theta}\sin\bar{\alpha}}{\sin(\bar{\theta}+\bar{\alpha})} \frac{1}{\bar{y}}$$

where $(^-)$ denotes the arithmetic mean for the characteristic increment in question, and these equations were solved by iterating until no significant change appeared in the values at a new point.

Calculations were made for two different mesh sizes, Δx_2 along the initial characteristic (Fig. 3) being taken as $0{\cdot}1$ and $0{\cdot}05$, and the results were extrapolated to zero mesh size by means of the ' deferred approach to the limit,' given by

$$f(0) = f(0{\cdot}05) + \tfrac{1}{3}[f(0{\cdot}05) - f(0{\cdot}10)] .$$

The correction $f(0) - f(0{\cdot}05)$ had of course to be interpolated at those points which had only been calculated with the smaller mesh.

I.2 *Integration of the Boundary Layer Equation.*—The stations used for integrating the differential equation (3.2.1) were :

$$x_1 = 0,\ 0{\cdot}05,\ 0{\cdot}10,\ 0{\cdot}15,\ 0{\cdot}20\ ;\ 0{\cdot}40,\ 0{\cdot}60,\ 0{\cdot}80\ ;\ 1{\cdot}20,\ 1{\cdot}60,\ 2{\cdot}00.$$

$$x_2 = 0,\ 0{\cdot}054,\ 0{\cdot}108,\ 0{\cdot}162,\ 0{\cdot}216\ ;\ 0{\cdot}324,\ 0{\cdot}432,\ 0{\cdot}540,\ 0{\cdot}648.$$

The values of x_1 were of course chosen to suit the pressure gradient over the parallel portion. The reason for choosing the values of x_2 was as follows.

The characteristics calculations gave values of α (and therefore of M, C_p, etc.) at unequal intervals along the body profiles, the intervals of x_2 being of the order of $0{\cdot}1$: the equally-spaced points $x_2 = 0,\ 0{\cdot}108, \ldots,\ 0{\cdot}648$, were chosen because they seemed the best means, towards the rear of the bodies, of the x_2-values at which the data was given.

Values of M at these points were obtained by means of Newton's interpolation formula for unequal intervals. Further values at $x_2 = 0{\cdot}054$ and $0{\cdot}162$ were then obtained so that the effect of the strong initial pressure gradient could be carefully observed.

The derivative dM_1/dx_2 was obtained by means of the four-strip formulae of Ref. 23. The equation (3.2.1) was integrated by using first the forward integration formulae and then the four-strip and three-strip formulae of Ref. 24, and iterations were made until no significant changes in ϑ and $d\vartheta/dx_1$ or $d\vartheta/dx_2$ appeared.

The total skin-friction integrals in equations (3.2.2) and (3.2.3) were also evaluated by the four-strip and three-strip formulae of Ref. 24.

I.3. *Evaluation of Afterbody Wave Drag Coefficients.*—The afterbody wave drag coefficient is defined by

$$C_D = \int_0^{l_2} C_p \frac{S'(x_2)}{S(0)}\, dx_2$$

$$= -\int_0^{l_2} C_p\, 4x_2(1 - x_2^2)\, dx_2 .$$

This coefficient, and the corresponding increment ΔC_D due to the displacement effect of the boundary layer were both calculated by means of the four-, five- and six-strip formulae of Ref. 24, the integration stations being $x_2 = 0,\ 0{\cdot}108,\ \ldots\ldots,\ 0{\cdot}648$.

I.4. *The Numerical Procedure in Applying the Method of Linearized Characteristics.*—In the linearized characteristics calculations, Δx_2 along the initial characteristic was taken as $0{\cdot}05$. In order to reduce the amount of labour by exploiting to the full the work of the original calculations, the original results for $\Delta x_2 = 0{\cdot}05$ were used, and not those depending on the deferred approach to the limit : the resulting error was certainly less than the error of $O(\alpha_1^2)$ due to the linearized method.

A great deal of interpolation of values at unequal intervals was required in these calculations, because the new boundary condition had to be applied at points off the original body (Fig. 3), so that $(\theta_0 + \theta_1)$ had first to be extrapolated slightly onto the original body, and at the end of the calculations $(\alpha_0 + \alpha_1)$ had to be interpolated back onto the modified body. These interpolations were performed by means of the Newton formula for unequal intervals along characteristics of the second family, as many strips, up to four, being used as were available : this procedure was consistent because initially, where only one or two strips were available, θ_0, θ_1, and the distance over which we were interpolating, were all extremely small.

Interpolation of the boundary condition along the modified body was also required. For this Bessel's formula for equal intervals was used, the coefficients being tabulated in Ref. 25.

APPENDIX II

Derivation of Log Law Formulae for the Turbulent Boundary Layer

The assumptions of section 3.1 regarding the compressible, turbulent boundary layer on a flat plate define the relations :

$$\frac{V}{V_{\tau w}} = \frac{1}{k} \log \frac{\eta V_{\tau w}}{a v_w}, \qquad \ldots\ldots\ldots\ldots\ldots\ldots\ldots\ldots \quad \text{(II.1)}$$

and $$\frac{T}{T_w} = 1 - c_1 \frac{V}{V_1} - c_2 \frac{V^2}{V_1^2},$$

where $$c_1 = 1 - \frac{T_{t1}}{T_w}, \qquad c_2 = \frac{T_{t1}}{T_w} \frac{M_1^2}{M_1^2 + 2/(\gamma - 1)}. \qquad \text{(II.2)}$$

Now $$\vartheta = \int_0^\delta \frac{\rho V}{\rho_1 V_1} \left(1 - \frac{V}{V_1}\right) d\eta,$$

and writing $V/V_1 = z$ we obtain

$$\frac{\rho}{\rho_1} = \frac{T_1}{T} = \frac{T_1}{T_w} \frac{1}{1 - c_1 z - c_2 z^2}, \qquad \text{(II.3)}$$

$$\eta = \exp\left(kz \frac{V_1}{V_{\tau w}}\right) \frac{a v_w}{V_{\tau w}}. \qquad \text{(II.4)}$$

Hence

$$\vartheta = \frac{T_1}{T_w} \cdot \frac{a v_w k V_1}{V_{\tau w}^2} \int_0^1 \frac{z(1-z)}{1 - c_1 z - c_2 z^2} \exp\left(k \frac{V_1}{V_{\tau w}} z\right) dz$$

$$= \frac{T_1}{T_w} \cdot \frac{a v_w k V_1}{V_{\tau w}^2} \cdot \frac{\exp(kV_1/V_{\tau w})}{(kV_1/V_{\tau w})^2 (1 - c_1 - c_2)} [1 + 0(V_{\tau w}/V_1)]$$

$$= \frac{a v_w}{k V_1} \exp(kV_1/V_{\tau w}) [1 + 0(V_{\tau w}/V_1)], \qquad \text{(II.5)}$$

which is equation (3.1.5).

Similarly

$$\delta^* = \int_0^\delta \left(1 - \frac{\rho V}{\rho_1 V_1}\right) d\eta$$

$$= \frac{a v_w k V_1}{V_{\tau w}^2} \int_0^1 \left[1 - \frac{(1 - c_1 - c_2) z}{1 - c_1 z - c_2 z^2}\right] \exp\left(k \frac{V_1}{V_{\tau w}} z\right) dz$$

$$= \frac{a v_w k V_1}{V_{\tau w}^2} \frac{(1 + c_2) \exp(kV_1/V_{\tau w})}{(1 - c_1 - c_2)(kV_1/V_{\tau w})^2} [1 + O(V_{\tau w}/V_1)]$$

$$= \frac{a v_w}{k V_1} \frac{1 + c_2}{1 - c_1 - c_2} \exp(kV_1/V_{\tau w}) [1 + O(V_{\tau w}/V_1)]. \qquad \text{(II.6)}$$

Thus $$H = \frac{\delta^*}{\vartheta} = \frac{1 + c_2}{1 - c_1 - c_2} [1 + O(V_{\tau w}/V_1)].$$

In the incompressible case $c_1 = c_2 = 0$ and $H_i \simeq 1{\cdot}0$, so that we may write

$$\frac{H}{H_i} = \frac{1 + c_2}{1 - c_1 - c_2}\,[1 + O(V_{\tau w}/V_1)]$$

$$= \left[\frac{T_w}{T_1} + \frac{\gamma - 1}{2}\,M_1^2\right]\left[1 + O(V_{\tau w}/V_1)\right], \qquad \text{(II.7)}$$

which is equation (3.1.6).

It remains to be shown that the constants C and D used by Squire and Young in the incompressible case can be taken over to compressible flow.

In the *incompressible* problem we have

$$\vartheta = \frac{\nu}{V_1}\,C e^{D\zeta}, \qquad \text{(II.8)}$$

where $$\zeta^2 = \frac{V_1^2}{V_\tau^2} = \frac{\rho V_1^2}{\tau_w} = \frac{2}{C_f},$$

and the momentum equation for a flat plate is

$$\frac{d\vartheta}{dx} = \frac{1}{\zeta^2} = \frac{C_f}{2}. \qquad \text{(II.9)}$$

Hence

$$C_F = \frac{1}{x}\int_0^x C_f\,dx = \frac{2\vartheta}{x}. \qquad \text{(II.10)}$$

Following Squire and Young, we assume that (II.8) is exact, and use (II.9) and (II.10) to transform it into a relation between C_F and R_e (the Reynolds number based on plate length), lower order terms in ζ being included. In (II.8) we have

$$\frac{d\vartheta}{dx} = \frac{\nu}{V_1}\,CDe^{D\zeta}\frac{d\zeta}{dx},$$

so that (II.9) becomes

$$\frac{\nu}{V_1}\,CDe^{D\zeta}\frac{d\zeta}{dx} = \frac{1}{\zeta^2} \qquad \text{(II.11)}$$

and hence $$\frac{V_1 x}{\nu} = R_e = Ce^{D\zeta}\left(\zeta^2 - \frac{2}{D}\,\zeta + \frac{2}{D^2}\right) - \frac{2C}{D^2}, \qquad \text{(II.12)}$$

where the constant of integration has been chosen to give $x = 0$ at $\zeta = 0$.

Again in (II.8)

$$\zeta = \frac{1}{D}\log\left(\frac{V_1\vartheta}{\nu C}\right)$$

by (II.10) $$= \frac{1}{D}\log\left(\frac{V_1 x C_F}{2\nu C}\right) = \frac{1}{D}\log\left(\frac{R_e C_F}{2C}\right). \qquad \text{(II.13)}$$

Hence (II.12) becomes

$$R_\theta = \frac{R_\theta C_F}{2}\left\{\left[\frac{1}{D}\log\left(\frac{R_\theta C_F}{2C}\right)\right]^2 - \frac{2}{D^2}\log\left(\frac{R_\theta C_F}{2C}\right) + \frac{2}{D^2}\right\} - \frac{2C}{D^2}. \quad \text{(II.14)}$$

The constants C and D were chosen by Squire and Young to make the relationship (II.14) between R_θ and C_F as similar to Prandtl's as possible.

In the *compressible* case we have

$$\vartheta = \frac{\nu_w}{V_1} C e^{D\zeta}, \quad \text{(II.15)}$$

$$\zeta^2 = \frac{V_1^2}{V_{\tau w}^2} = \frac{\rho_w V_1^2}{\tau_w} = \frac{2}{C_{f w}},$$

and

$$\frac{d\vartheta}{dx} = \frac{1}{\zeta^2}\frac{\rho_w}{\rho_1} = \frac{C_f}{2}. \quad \text{(II.16)}$$

Hence

$$C_F = \frac{1}{x}\int_0^x C_f\, dx = \frac{2\vartheta}{x}. \quad \text{(II.17)}$$

In place of (II.11) we have

$$\frac{\nu_w}{V_1} \cdot CD e^{D\zeta}\frac{d\zeta}{dx} = \frac{1}{\zeta^2}\frac{\rho_w}{\rho_1} \quad \text{(II.18)}$$

and hence

$$\frac{V_1 x}{\nu_w}\frac{\rho_w}{\rho_1} = R_{\theta w}\frac{T_1}{T_w} = C e^{D\zeta}\left(\zeta^2 - \frac{2}{D}\zeta + \frac{2}{D^2}\right) - \frac{2C}{D^2}. \quad \text{(II.19)}$$

In place of (II.13) we have

$$\zeta = \frac{1}{D}\log\left(\frac{V_1\vartheta}{\nu_w C}\right)$$

$$= \frac{1}{D}\log\left(\frac{V_1 x C_F}{2\nu_w C}\right) = \frac{1}{D}\log\left(\frac{R_{\theta w} C_{F w}}{2C}\cdot\frac{T_1}{T_w}\right). \quad \text{(II.20)}$$

Thus $R_{\theta w}T_1/T_w$ and $C_{F w}$ in equations (II.19) and (II.20) have exactly replaced R_θ and C_F in equations (II.12) and (II.13) ; and the problem of finding the best C and D for agreement with the extension of Prandtl's formula (in which R_θ and C_F have also been replaced by $R_{\theta w}T_1/T_w$ and $C_{F w}$) is the same as in the incompressible case.

APPENDIX III

The Compatibility Equations of the Linearized Characteristics Method in Isentropic, Axially Symmetric Flow

For isentropic, axially symmetric flow Ferri's compatibility equations are[18] :

for C_1

$$\frac{1}{V_0}\frac{dV_1}{dx} - \tan\alpha_0\frac{d\theta_1}{dx}$$

$$+\left[\tan\alpha_0\frac{\sin(\theta_0-\alpha_0)}{\cos(\theta_0+\alpha_0)}\frac{1}{y} - \frac{1}{V_0}\left(\frac{dV_0}{dx}\right)_{(2)}\frac{2\cos(\theta_0-\alpha_0)}{\sin 2\alpha_0\cos(\theta_0+\alpha_0)}\right]\theta_1$$

$$+\left[\frac{1}{V_0}\frac{dV_0}{dx}\tan^2\alpha_0\left(1+\frac{\gamma-1}{2\sin^4\alpha_0}\right)\right.$$

$$\left.+\frac{1}{V_0}\left(\frac{dV_0}{dx}\right)_{(2)}\frac{\cos(\theta_0-\alpha_0)}{\cos(\theta_0+\alpha_0)}\frac{1}{\cos^2\alpha_0}\left(1+\frac{\gamma-1}{2\sin^2\alpha_0}\right)\right]\frac{V_1}{V_0}=0, \quad .. \quad \text{(III.1)}$$

and for C_2

$$\frac{1}{V_0}\frac{dV_1}{dx} + \tan\alpha_0\frac{d\theta_1}{dx}$$

$$-\left[\tan\alpha_0\frac{\sin(\theta_0+\alpha_0)}{\cos(\theta_0-\alpha_0)}\frac{1}{y} - \frac{1}{V_0}\left(\frac{dV_0}{dx}\right)_{(1)}\frac{2\cos(\theta_0+\alpha_0)}{\sin 2\alpha_0\cos(\theta_0-\alpha_0)}\right]\theta_1$$

$$+\left[\frac{1}{V_0}\frac{dV_0}{dx}\tan^2\alpha_0\left(1+\frac{\gamma-1}{2\sin^4\alpha_0}\right)\right.$$

$$\left.+\frac{1}{V_0}\left(\frac{dV_0}{dx}\right)_{(1)}\frac{\cos(\theta_0+\alpha_0)}{\cos(\theta_0-\alpha_0)}\frac{1}{\cos^2\alpha_0}\left(1+\frac{\gamma-1}{2\sin^2\alpha_0}\right)\right]\frac{V_1}{V_0}=0, \quad .. \quad \text{(III.2)}$$

where V_0, θ_0 and α_0 are, respectively, the magnitude and inclination of the velocity vector and the Mach angle in the original flow field, and $(V_0 + V_1)$ and $(\theta_0 + \theta_1)$ are the magnitude and direction of the velocity vector in the new flow.

Now writing $V/a_t = \tilde{V}$, where a_t is the velocity of sound at stagnation conditions, we have from the energy equation

$$\frac{1}{\tilde{V}_0^2} = \frac{\gamma-1}{2} + \sin^2\alpha_0\,, \quad .. \quad .. \quad .. \quad .. \quad .. \quad .. \quad .. \quad \text{(III.3a)}$$

$$\frac{1}{(\tilde{V}_0+\tilde{V}_1)^2} = \frac{\gamma-1}{2} + \sin^2(\alpha_0+\alpha_1), \quad .. \quad .. \quad .. \quad .. \quad .. \quad .. \quad \text{(III.3b)}$$

hence

$$\frac{\tilde{V}_1}{\tilde{V}_0^3} = -\alpha_1\sin\alpha_0\cos\alpha_0 + 0(\alpha_1^2). \quad .. \quad .. \quad .. \quad .. \quad .. \quad .. \quad \text{(III.4)}$$

Writing

$$\frac{\gamma-1}{2} + \sin^2\alpha_0 = \psi$$

we have

$$\tilde{V}_0 = \psi^{-1/2},$$

$$d\tilde{V}_0 = -\tfrac{1}{2}\psi^{-3/2}\sin 2\alpha_0\, d\alpha_0,$$

$$\tilde{V}_1 = -\tfrac{1}{2}\alpha_1\psi^{-3/2}\sin 2\alpha_0,$$

$$d\tilde{V}_1 = -\tfrac{1}{2}\psi^{-3/2}\sin 2\alpha_0\, d\alpha_1 - \tfrac{1}{2}\alpha_1[-\tfrac{3}{2}\psi^{-5/2}\sin^2 2\alpha_0 + \psi^{-3/2}\,2\cos 2\alpha_0]d\alpha_0,$$

$$\frac{\tilde{V}_1}{\tilde{V}_0} = \frac{V_1}{V_0} \doteq -\tfrac{1}{2}\alpha_1\psi^{-1}\sin 2\alpha_0, \qquad \text{(III.5)}$$

$$\frac{dV_0}{V_0} = -\tfrac{1}{2}\psi^{-1}\sin 2\alpha_0\, d\alpha_0, \qquad \text{(III.6)}$$

$$\frac{dV_1}{V_0} = -\tfrac{1}{2}\psi^{-1}\sin 2\alpha_0\, d\alpha_1 - \tfrac{1}{2}\alpha_1[-\tfrac{3}{2}\psi^{-2}\sin^2 2\alpha_0 + \psi^{-1}\,2\cos 2\alpha_0]d\alpha_0. \qquad \text{(III.7)}$$

Upon substitution of (III.5), (III.6), (III.7) and the relations

$$\frac{dy}{dx} = \tan(\theta_0 \pm \alpha_0),$$

and after considerable reduction, the compatibility equations (III.1), (III.2), become those in the main text, namely

for C_1

$$\frac{d\alpha_1}{dy} + D_1\frac{d\theta_1}{dy} - (D_1F_1 + E_1)\theta_1 - \left(G_1\frac{d\alpha_0}{dy} + E_1\right)\alpha_1 = 0, \qquad \text{(III.8)}$$

for C_2

$$\frac{d\alpha_1}{dy} - D_2\frac{d\theta_1}{dy} + (D_2F_2 + E_2)\theta_1 - \left(G_2\frac{d\alpha_0}{dy} + E_2\right)\alpha_1 = 0, \qquad \text{(III.9)}$$

where

$$D_1 = D_2 = \frac{2\sin^2\alpha_0 + \gamma - 1}{2\cos^2\alpha_0},$$

$$E_1 = \left(\frac{d\alpha_0}{dy}\right)_{(2)}\frac{2\sin(\theta_0 - \alpha_0)}{\sin 2\alpha_0\sin(\theta_0 + \alpha_0)}, \qquad E_2 = \left(\frac{d\alpha_0}{dy}\right)_{(1)}\frac{2\sin(\theta_0 + \alpha_0)}{\sin 2\alpha_0\sin(\theta_0 - \alpha_0)},$$

$$F_1 = \frac{\sin(\theta_0 - \alpha_0)}{\sin(\theta_0 + \alpha_0)}\frac{1}{y}, \qquad F_2 = \frac{\sin(\theta_0 + \alpha_0)}{\sin(\theta_0 - \alpha_0)}\frac{1}{y},$$

$$G_1 = G_2 = \tan\alpha_0\frac{2(\gamma + 1)}{2\sin^2\alpha_0 + \gamma - 1}.$$

α_1 and θ_1 can obviously be in degrees, but α_0 must be in radians.

In applying the method, the coefficients D_1, E_1, etc., and also the coefficients p_1, q_1, etc., below, may be evaluated in terms of $\bar{\theta}_0$, $\bar{\alpha}_0$, and $\bar{y}$, the arithmetic means for each strip ; the derivatives in E_1 and E_2 can be evaluated by averaging the values of $\Delta\alpha/\Delta y$ on the strips on either side of, and of opposite family to, the strip in question. This last step is consistent with the order of accuracy of the calculations only if the difference in length of adjacent characteristic strips of the same family is $O(\Delta y^2)$; this condition was satisfied in the present case.

It is worth noting that in a field of finite extent considerably less labour is required to evaluate the coefficients immediately in terms of mean values $\bar{\theta}_0$, $\bar{\alpha}_0$ and $\bar{y}$, than is required to evaluate the coefficients at all the intersection points in the field, and then to calculate mean values of these coefficients on the strips : the accuracy, as predicted by mathematical order arguments, is the same for the two methods.

To proceed from a point A, where (α_1, θ_1) are known, to a point C where (α_1, θ_1) are unknown, by means of a characteristic strip of the first family, we replace the differential equation (III.8) by the following difference equation :

$$(\alpha_{1C} - \alpha_{1A}) + D_1(\theta_{1C} - \theta_{1A}) - (D_1F_1 + E_1) \cdot \tfrac{1}{2}(\theta_{1C} + \theta_{1A}) \cdot (y_C - y_A)$$
$$- [(\alpha_{0C} - \alpha_{0A})G_1 + E_1(y_C - y_A)] \cdot \tfrac{1}{2}(\alpha_{1C} + \alpha_{1A}) = 0. \quad .. \quad .. \quad \text{(III.10)}$$

This may be written

$$\alpha_{1C} = p_1\alpha_{1A} + q_1\theta_{1A} - r_1\theta_{1C}, \quad .. \quad .. \quad .. \quad .. \quad .. \quad .. \quad \text{(III.11)}$$

where

$$m_1 = \tfrac{1}{2}[(\alpha_{0C} - \alpha_{0A})G_1 + E_1(y_C - y_A)],$$
$$n_1 = \tfrac{1}{2}(D_1F_1 + E_1)(y_C - y_A),$$
$$p_1 = \frac{1 + m_1}{1 - m_1},$$
$$q_1 = \frac{D_1 + n_1}{1 - m_1},$$
$$r_1 = \frac{D_1 - n_1}{1 - m_1},$$

Similarly, for a strip BC of a second family characteristic we obtain

$$\alpha_{1C} = p_2\alpha_{1B} - q_2\theta_{1B} + r_2\theta_{1C}, \quad .. \quad .. \quad .. \quad .. \quad .. \quad .. \quad \text{(III.12)}$$

where

$$m_2 = \tfrac{1}{2}[(\alpha_{0C} - \alpha_{0B})G_2 + E_2(y_C - y_B)]$$
$$n_2 = \tfrac{1}{2}(D_2F_2 + E_2)(y_C - y_B),$$
$$p_2 = \frac{1 + m_2}{1 - m_2},$$
$$q_2 = \frac{D_2 + n_2}{1 - m_2},$$
$$r_2 = \frac{D_2 - n_2}{1 - m_2}.$$

When θ_{1C} is given by the boundary condition (III.11) or (III.12) are used, but for a point within the field the two are solved simultaneously, so that

$$\theta_{1C} = \frac{1}{r_1 + r_2}[p_1\alpha_{1A} + q_1\theta_{1A} - p_2\alpha_{1B} + q_2\theta_{1B}]. \quad .. \quad .. \quad .. \quad .. \quad \text{(III.13)}$$

An analysis of the above procedure of the type given in Refs. 8 and 18 shows that the error is the larger of

$$O(\alpha_1^2) \text{ and } O(\alpha_1 \Delta y^3),$$

the former being inherent in the theory of linearized characteristics. In principle the error represented by the second O-term cannot be reduced by iteration or by a more complicated procedure, but only by tightening the mesh.

More particular details of the numerical procedure used in the present case are given in Appendix I.

TABLE 1

Flows Along the Parallel Portion

x_1	M_1	$-C_p$	$-\frac{1}{V_1}\frac{dV_1}{dx_1}$	ϑ (in.)	δ^* (in.)	$\frac{d\vartheta}{dx_1}$ (in.)	$\frac{d\delta^*}{dx_1}$ (in.)	C_f
				(*a*) $M_0 = 1{\cdot}2$				
0	1·4116	0·2484	0·9071	0·0020	0·0048	0·0384	0·0871	0·00344
0·05	1·3440	0·1746	0·5530	0·0038	0·0088	0·0348	0·0750	0·00299
0·10	1·3049	0·1296	0·3489	0·0055	0·0124	0·0323	0·0685	0·00278
0·15	1·2801	0·1001	0·2275	0·0071	0·0157	0·0303	0·0638	0·00264
0·20	1·2463	0·0809	0·1539	0·0085	0·0189	0·0286	0·0603	0·00255
0·40	1·2336	0·0428	0·0699	0·0139	0·0302	0·0256	0·0534	0·00232
0·60	1·2187	0·0240	0·0303	0·0188	0·0403	0·0233	0·0489	0·00220
0·80	1·2118	0·0152	0·0154	0·0233	0·0498	0·0219	0·0463	0·00212
1·20	1·2060	0·0077	0·0055	0·0317	0·0676	0·0203	0·0429	0·00202
1·60	1·2036	0·0046	0·0026	0·0397	0·0843	0·0193	0·0409	0·00193
2·00	1·2024	0·0031	0·0014	0·0472	0·1003	0·0187	0·0395	0·00187
				(*b*) $M_0 = 1{\cdot}4$				
0	1·5822	0·1686	0·4382	0·0018	0·0049	0·0342	0·0878	0·00328
0·05	1·5394	0·1323	0·3096	0·0034	0·0089	0·0304	0·0748	0·00284
0·10	1·5099	0·1061	0·2242	0·0049	0·0125	0·0286	0·0691	0·00264
0·15	1·4890	0·0869	0·1659	0·0063	0·0158	0·0272	0·0649	0·00251
0·20	1·4736	0·0725	0·1254	0·0076	0·0190	0·0261	0·0620	0·00241
0·40	1·4397	0·0399	0·0554	0·0126	0·0306	0·0234	0·0549	0·00220
0·60	1·4238	0·0241	0·0278	0·0171	0·0412	0·0217	0·0510	0·00207
0·80	1·4155	0·0157	0·0153	0·0213	0·0511	0·0205	0·0484	0·00193
1·20	1·4079	0·0081	0·0058	0·0291	0·0697	0·0190	0·0451	0·00188
1·60	1·4048	0·0049	0·0028	0·0366	0·0874	0·0181	0·0431	0·00181
2·00	1·4032	0·0033	0·0015	0·0437	0·1043	0·0175	0·0416	0·00175
				(*c*) $M_0 = 1{\cdot}6$				
0	1·7720	0·1272	0·2787	0·0017	0·0050	0·0317	0·0918	0·00312
0·05	1·7381	0·1044	0·2107	0·0032	0·0092	0·0277	0·0775	0·00269
0·10	1·7126	0·0865	0·1613	0·0045	0·0129	0·0261	0·0715	0·00249
0·15	1·6934	0·0727	0·1251	0·0058	0·0164	0·0248	0·0671	0·00237
0·20	1·6788	0·0619	0·0984	0·0070	0·0197	0·0239	0·0642	0·00228
0·40	1·6449	0·0361	0·0431	0·0115	0·0317	0·0215	0·0571	0·00207
0·60	1·6285	0·0231	0·0241	0·0157	0·0427	0·0201	0·0533	0·00195
0·80	1·6193	0·0157	0·0143	0·0196	0·0532	0·0191	0·0508	0·00187
1·20	1·6101	0·0083	0·0058	0·0270	0·0728	0·0178	0·0475	0·00177
1·60	1·6062	0·0051	0·0029	0·0339	0·0913	0·0170	0·0454	0·00170
0·20	1·6041	0·0034	0·0016	0·0406	0·1092	0·0164	0·0439	0·00164

TABLE 2

Flows Along the Afterbodies

x_2	M_1	$-C_p$	$\frac{1}{V_1}\frac{dV_1}{dx_2}$	ϑ (in.)	δ^* (in.)	$\frac{d\vartheta}{dx_2}$ (in.)	$\frac{d\delta^*}{dx_2}$ (in.)	C_f	ΔC_p†
				(*a*) $t = 0{\cdot}1$, $M_0 = 1{\cdot}2$					
0	1·2000	0	0·2850	0·0472	0·1002	−0·0130	−0·0025	0·00187	−0·0003
0·054	1·2204	0·0262	0·2007	0·0470	0·1008	+0·0031	+0·0248	0·00186	
0·108	1·2350	0·0446	0·1437	0·0475	0·1029	0·0153	0·0467	0·00185	+0·0034
0·162	1·2458	0·0581	0·1042	0·0486	0·1058	0·0256	0·0661	0·00184	
0·216	1·2537	0·0679	0·0758	0·0503	0·1099	0·0354	0·0853	0·00183	0·0042
0·324	1·2634	0·0798	+0·0320	0·0552	0·1214	0·0576	0·1326	0·00179	0·0044
0·432	1·2653	0·0821	−0·0112	0·0631	0·1389	0·0905	0·1978	0·00175	0·0046
0·540	1·2591	0·0745	−0·0601	0·0756	0·1658	0·1483	0·3157	0·00170	0·0059
0·648	1·2427	0·0542	−0·1293	0·0974	0·2117	0·2711	0·5636	0·00163	0·0101
				(*b*) $t = 0{\cdot}1$, $M_0 = 1{\cdot}4$					
0	1·4000	0	0·2105	0·0437	0·1041	−0·0006	0·0238	0·00175	0·0020
0·054	1·4189	0·0196	0·1534	0·0440	0·1059	+0·0102	0·0436	0·00175	
0·108	1·4335	0·0337	0·1188	0·0448	0·1087	0·0186	0·0607	0·00173	0·0035
0·162	1·4452	0·0452	0·0960	0·0460	0·1124	0·0262	0·0772	0·00172	
0·216	1·4545	0·0543	0·0732	0·0476	0·1171	0·0346	0·0955	0·00171	0·0038
0·324	1·4671	0·0663	0·0379	0·0523	0·1297	0·0540	0·1400	0·00167	0·0040
0·432	1·4719	0·0709	+0·0034	0·0596	0·1482	0·0831	0·2073	0·00164	0·0043
0·540	1·4682	0·0673	−0·0363	0·0710	0·1761	0·1340	0·3243	0·00159	0·0053
0·648	1·4547	0·0545	−0·0852	0·0905	0·2225	0·2393	0·5652	0·00153	0·0087
				(*c*) $t = 0{\cdot}1$, $M_0 = 1{\cdot}6$					
0	1·6000	0	0·1592	0·0406	0·1089	0·0067	0·0429	0·00165	0·0028
0·054	1·6189	0·0154	0·1283	0·0411	0·1116	0·0137	0·0582	0·00163	
0·108	1·6344	0·0279	0·1036	0·0421	0·1152	0·0203	0·0734	0·00162	0·0036
0·162	1·6472	0·0378	0·0850	0·0433	0·1196	0·0268	0·0895	0·00161	
0·216	1·6579	0·0461	0·0691	0·0450	0·1249	0·0339	0·1073	0·00160	0·0036
0·324	1·6733	0·0577	0·0410	0·0495	0·1388	0·0512	0·1523	0·00157	0·0037
0·432	1·6808	0·0634	+0·0117	0·0564	0·1587	0·0775	0·2211	0·00153	0·0041
0·540	1·6794	0·0624	−0·0238	0·0669	0·1882	0·1237	0·3407	0·00148	0·0050
0·648	1·6666	0·0527	−0·0676	0·0850	0·2367	0·2189	0·5858	0·00143	0·0078
				(*d*) $t = 0{\cdot}1414$, $M_0 = 1{\cdot}2$					
0	1·2000	0	0·4226	0·0472	0·1002	−0·0372	−0·0418	0·00187	−0·0071
0·054	1·2305	0·0389	0·3026	0·0459	0·0990	−0·0154	−0·0058	0·00186	
0·108	1·2537	0·0679	0·2320	0·0454	0·0994	−0·0138	+0·0188	0·00186	+0·0030
0·162	1·2722	0·0905	0·1839	0·0457	0·1009	+0·0096	0·0393	0·00185	
0·214	1·2869	0·1082	0·1404	0·0465	0·1036	0·0204	0·0598	0·00184	0·0055
0·324	1·3071	0·1321	0·0747	0·0498	0·1123	0·0424	0·1043	0·00181	0·0067
0·432	1·3153	0·1417	+0·0115	0·0559	0·1268	0·0733	0·1677	0·00177	0·0076
0·540	1·3104	0·1360	−0·0662	0·0664	0·1501	0·1277	0·2783	0·00172	0·0099
0·648	1·2881	0·1096	−0·1789	0·0858	0·1913	0·2457	0·5141	0·00165	0·0172

† ΔC_p is the increment in pressure coefficient due to the boundary-layer displacement effect.

TABLE 2—*continued*

Flows Along the Afterbodies

x_2	M_1	$-C_p$	$\frac{1}{V_2}\frac{dV_1}{dx_2}$	ϑ (in.)	δ^* (in.)	$\frac{d\vartheta}{dx_2}$ (in.)	$\frac{d\delta^*}{dx_2}$ (in.)	C_f	ΔC_p
				$(e)\ t = 0{\cdot}1414,\ M_0 = 1{\cdot}4$					
0	1·4000	0	0·2809	0·0437	0·1041	−0·0144	−0·0007	0·00175	−0·0001
0·054	1·4275	0·0278	0·2337	0·0432	0·1046	−0·0041	+0·0191	0·00175	
0·108	1·4506	0·0505	0·1897	0·0432	0·1061	+0·0054	0·0380	0·00174	+0·0038
0·162	1·4700	0·0691	0·1545	0·0438	0·1086	0·0140	0·0357	0·00173	
0·216	1·4863	0·0843	0·1279	0·0447	0·1121	0·0221	0·0738	0·00171	0·0052
0·324	1·5105	0·1066	0·0790	0·0481	0·1223	0·0410	0·1170	0·00168	0·0060
0·432	1·5236	0·1183	+0·0296	0·0539	0·1381	0·0682	0·1801	0·00165	0·0069
0·540	1·5238	0·1185	−0·0312	0·0635	0·1627	0·1154	0·2890	0·00160	0·0088
0·648	1·5067	0·1031	−0·1175	0·0807	0·2047	0·2154	0·5152	0·00154	0·0145
				$(f)\ t = 0{\cdot}1414,\ M_0 = 1{\cdot}6$					
0	1·6000	0	0·2286	0·0406	0·1089	−0·0053	0·0218	0·00165	0·0020
0·054	1·6275	0·0223	0·1898	0·0405	0·1105	+0·0027	0·0387	0·00164	
0·108	1·6514	0·0411	0·1617	0·0409	0·1131	0·0097	0·0547	0·00163	0·0045
0·162	1·6723	0·0570	0·1385	0·0416	0·1165	0·0164	0·0712	0·00161	
0·216	1·6903	0·0705	0·1169	0·0427	0·1208	0·0235	0·0890	0·00160	0·0051
0·324	1·7188	0·0910	0·0782	0·0461	0·1326	0·0402	0·1327	0·00157	0·0057
0·432	1·7362	0·1031	+0·0378	0·0516	0·1502	0·0646	0·1975	0·00153	0·0065
0·540	1·7404	0·1060	−0·0119	0·0606	0·1768	0·1070	0·3085	0·00149	0·0082
0·648	1·7269	0·0966	−0·0815	0·0763	0·2209	0·1952	0·5351	0·00144	0·0127
				$(g)\ t = 0{\cdot}2,\ M_0 = 1{\cdot}2$					
0	1·2000	0	0·5855	0·0472	0·1002	−0·0626	−0·0814	0·00187	−0·0195
0·054	1·2442	0·0561	0·4513	0·0446	0·0970	−0·0365	−0·0387	0·00187	
0·108	1·2802	0·1001	0·3562	0·0431	0·0958	−0·0187	−0·0080	0·00186	−0·0019
0·162	1·3102	0·1358	0·2888	0·0425	0·0961	−0·0056	+0·0158	0·00186	
0·216	1·3356	0·1651	0·2362	0·0425	0·0975	+0·0055	0·0370	0·00185	+0·0052
0·324	1·3740	0·2080	0·1482	0·0442	0·1038	0·0272	0·0810	0·00182	0·0090
0·432	1·3957	0·2315	+0·0606	0·0486	0·1155	0·0556	0·1402	0·00178	0·0118
0·540	1·3979	0·2339	−0·0457	0·0569	0·1354	0·1040	0·2404	0·00173	0·0160
0·648	1·3736	0·2076	−0·1990	0·0731	0·1714	0·2097	0·4538	0·00166	0·0281
				$(h)\ t = 0{\cdot}2,\ M_0 = 1{\cdot}4$					
0	1·4000	0	0·4142	0·0437	0·1041	−0·0330	−0·0291	0·00175	−0·0048
0·054	1·4401	0·0402	0·3364	0·0423	0·1033	−0·0183	−0·0027	0·00175	
0·108	1·4748	0·0736	0·2857	0·0416	0·1037	−0·0077	+0·0181	0·00174	+0·0015
0·162	1·5056	0·1021	0·2468	0·0415	0·1052	+0·0013	0·0371	0·00173	
0·216	1·5328	0·1264	0·2091	0·0418	0·1077	0·0101	0·0563	0·00172	0·0056
0·324	1·5767	0·1640	0·1433	0·0438	0·1159	0·0287	0·0993	0·00169	0·0083
0·432	1·6053	0·1875	+0·0771	0·0482	0·1297	0·0537	0·1590	0·00165	0·0105
0·540	1·6156	0·1956	−0·0342	0·0560	0·1517	0·0959	0·2590	0·00160	0·0139
0·648	1·6002	0·1833	−0·1211	0·0706	0·1894	0·1857	0·4650	0·00154	0·0230

TABLE 2—*continued*

Flows Along the Afterbodies

x_2	M_1	$-C_p$	$\frac{1}{V_1}\frac{dV_1}{dx_2}$	ϑ (in.)	δ^* (in.)	$\frac{d\vartheta}{dx_2}$ (in.)	$\frac{d\delta^*}{dx_2}$ (in.)	C_f	ΔC_p
				(*i*) $t = 0{\cdot}2$, $M_0 = 1{\cdot}6$					
0	1·6000	0	0·3222	0·0406	0·1089	−0·0176	0·0036	0·00165	0·0005
0·054	1·6397	0·0320	0·2763	0·0399	0·1096	−0·0082	0·0230	0·00164	
0·108	1·6756	0·0595	0·2425	0·0397	0·1114	−0·0005	0·0409	0·00163	0·0039
0·162	1·7083	0·0835	0·2134	0·0399	0·1141	+0·0067	0·0587	0·00161	
0·216	1·7377	0·1042	0·1860	0·0404	0·1177	0·0140	0·0773	0·00160	0·0061
0·324	1·7874	0·1372	0·1359	0·0428	0·1283	0·0302	0·1212	0·00157	0·0078
0·432	1·8227	0·1593	0·0823	0·0472	0·1445	0·0529	0·1837	0·00153	0·0097
0·540	1·8396	0·1696	0·0165	0·0547	0·1694	0·0913	0·2877	0·00149	0·0126
0·648	1·8308	0·1643	−0·0741	0·0683	0·2104	0·1705	0·4966	0·00143	0·0196

TABLE 3

Afterbody Wave Drag Coefficients

C_D = Wave drag coefficient in inviscid flow, based on maximum cross-section area.
ΔC_D = Change in the wave drag coefficient due to the presence of the boundary layer.

l_2	$M_0 = 1{\cdot}2$		$M_0 = 1{\cdot}4$		$M_0 = 1{\cdot}6$	
	C_D	ΔC_D	C_D	ΔC_D	C_D	ΔC_D
			(*a*) $t = 0{\cdot}1$			
0·108	0·0008	−0·0001	0·0006	−0·0001	0·0005	−0·0001
0·216	0·0047	−0·0003	0·0037	−0·0003	0·0031	−0·0003
0·324	0·0128	−0·0008	0·0103	−0·0007	0·0088	−0·0007
0·432	0·0242	−0·0014	0·0199	−0·0013	0·0173	−0·0013
0·540	0·0369	−0·0022	0·0311	−0·0021	0·0274	−0·0020
0·648	0·0477	−0·0035	0·0413	−0·0032	0·0371	−0·0030
			(*b*) $t = 0{\cdot}1414$			
0·108	0·0011	0	0·0008	−0·0001	0·0007	−0·0001
0·216	0·0074	−0·0003	0·0056	−0·0004	0·0046	−0·0004
0·324	0·0205	−0·0010	0·0161	−0·0010	0·0135	−0·0010
0·432	0·0398	−0·0020	0·0319	−0·0019	0·0271	−0·0019
0·540	0·0622	−0·0034	0·0510	−0·0031	0·0439	−0·0030
0·648	0·0828	−0·0055	0·0695	−0·0050	0·0609	−0·0047
			(*c*) $t = 0{\cdot}2$			
0·108	0·0017	+0·0001	0·0012	0	0·0010	−0·0001
0·216	0·0110	0	0·0083	−0·0003	0·0067	−0·0004
0·324	0·0315	−0·0008	0·0242	−0·0010	0·0200	−0·0012
0·432	0·0624	−0·0023	0·0489	−0·0023	0·0408	−0·0024
0·540	0·0999	−0·0045	0·0797	−0·0043	0·0673	−0·0042
0·648	0·1368	−0·0079	0·1113	−0·0071	0·0951	−0·0067

TABLE 4

Total Skin-friction Coefficients

(a) Parallel portion

M_0	Body C_F	Flat plate C_F	
		For R_e based on distance from nose	For R_e based on distance from shoulder
1·2	0·00217	0·00204	0·00217
1·4	0·00202	0·00190	0·00203
1·6	0·00189	0·00178	0·00190

(b) Parallel portion + afterbody

t	M_0	Body C_F	Flat plate C_F	
			For R_e based on distance from nose	For R_e based on distance from shoulder
0·1	1·2	0·00203	0·00196	0·00206
	1·4	0·00189	0·00183	0·00193
	1·6	0·00176	0·00172	0·00179
0·1414	1·2	0·00206	0·00200	0·00210
	1·4	0·00192	0·00186	0·00196
	1·6	0·00178	0·00174	0·00183
0·2	1·2	0·00209	0·00201	0·00211
	1·4	0·00194	0·00185	0·00197
	1·6	0·00180	0·00175	0·00184

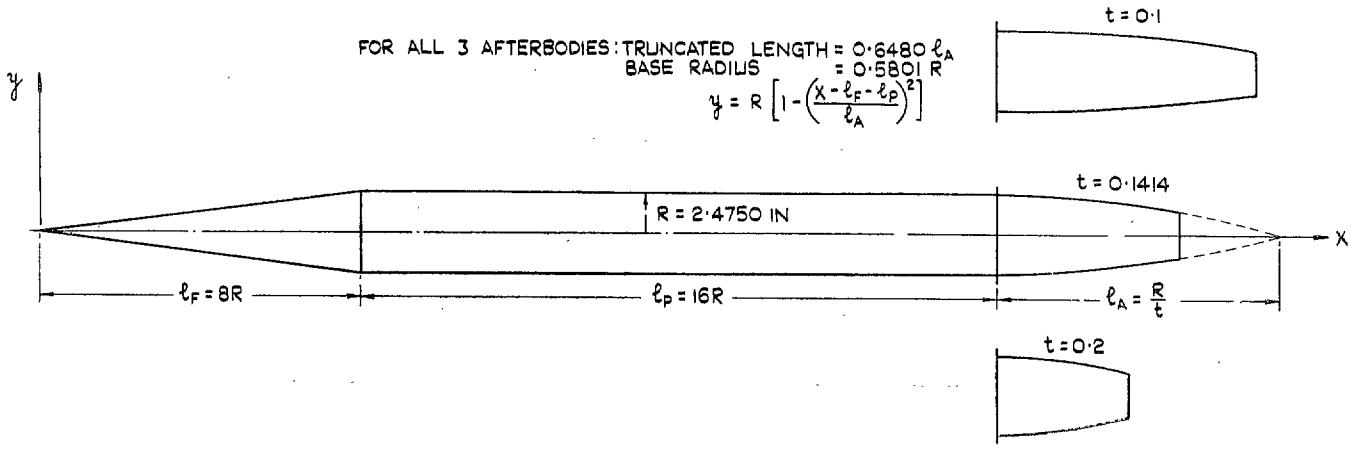

FIG. 1. The bodies of revolution.

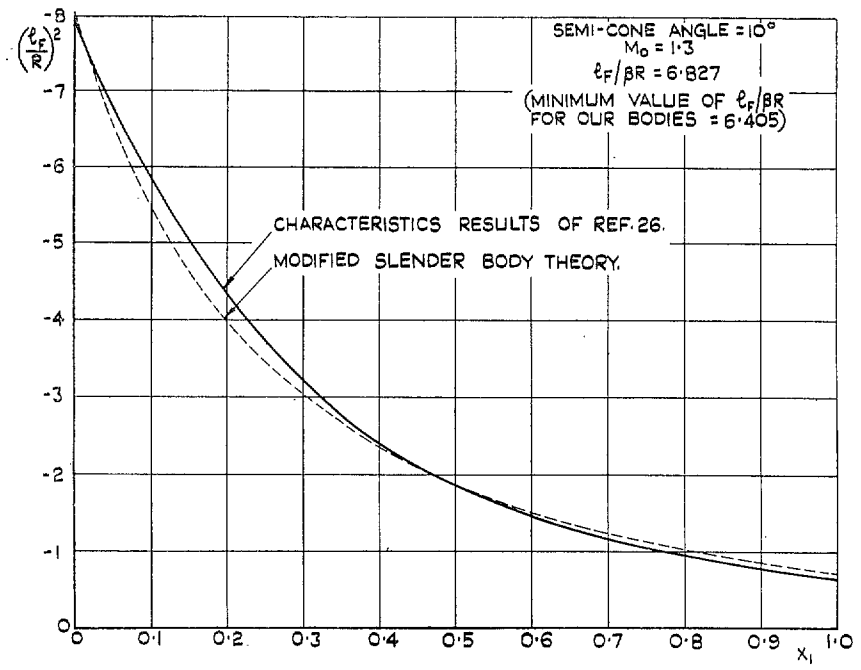

FIG. 2. Comparison of exact and approximate results for the pressures on a parallel portion.

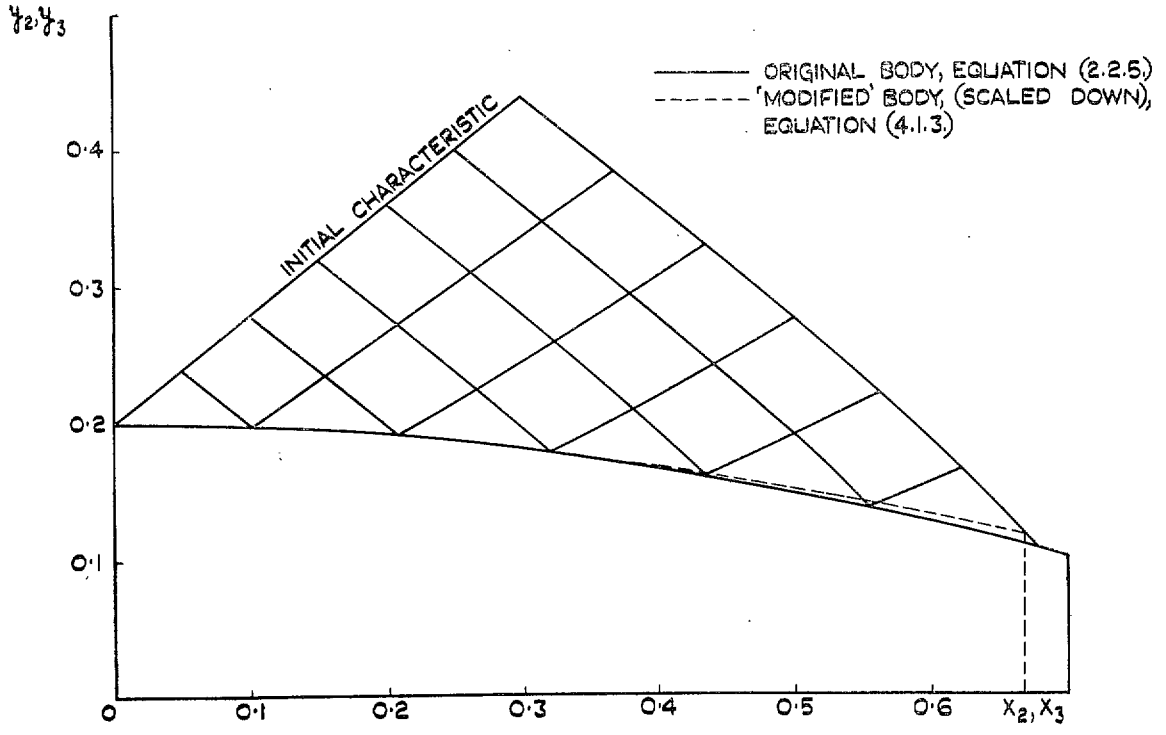

FIG. 3. Characteristics network for $t = 0{\cdot}2$, $M_0 = 1{\cdot}6$.

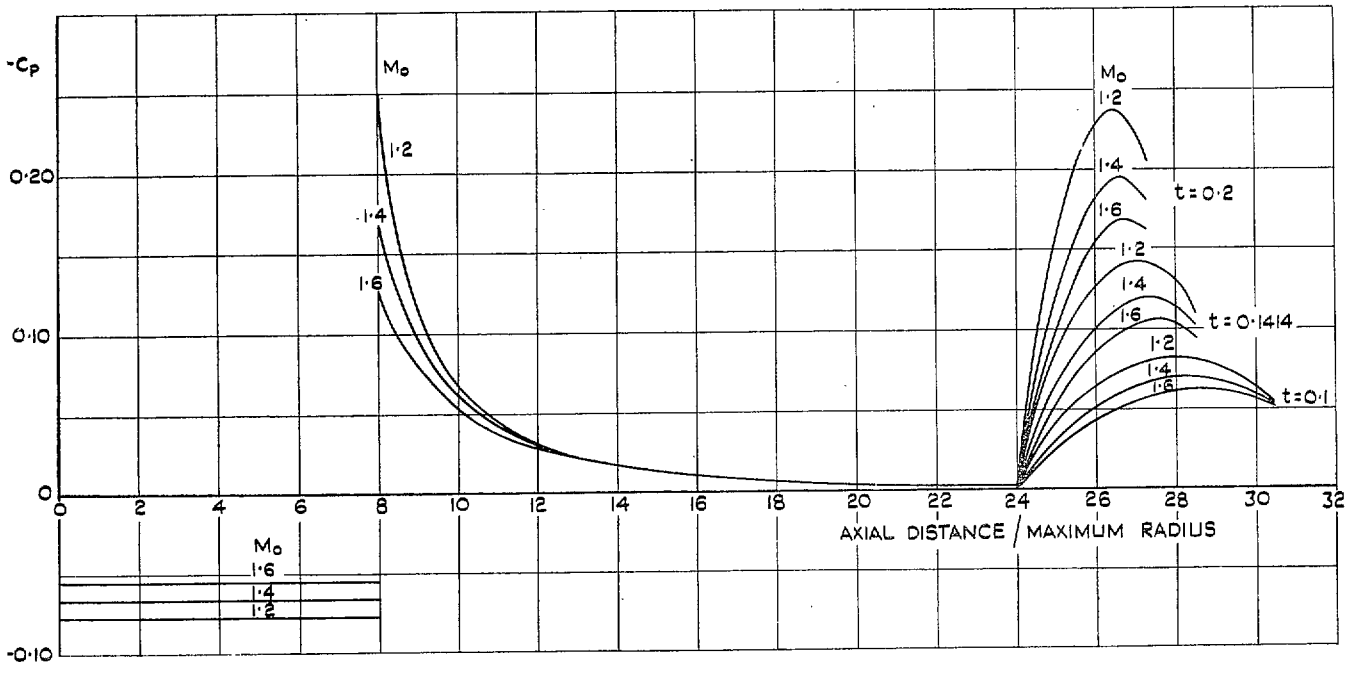

FIG. 4. Pressure distributions on the bodies in inviscid flow.

$C_{P_{MIN}}$ = COEFFICIENT CORRESPONDING TO MINIMUM PRESSURE ON AN AFTERBODY IN INVISCID FLOW.

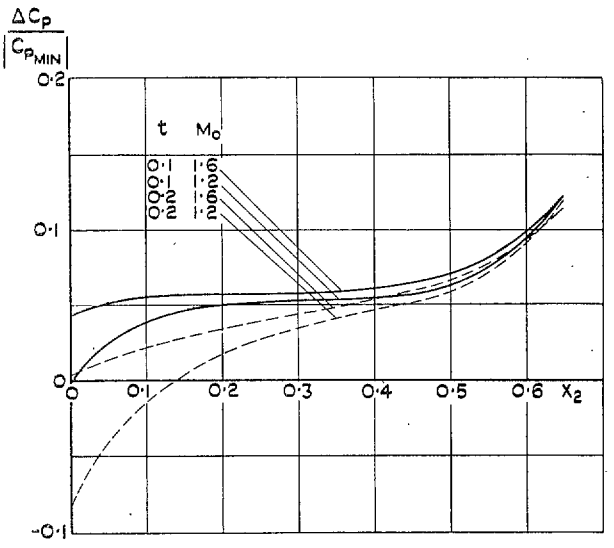

FIG. 5. Changes in the afterbody pressure coefficients due to the presence of boundary layers.

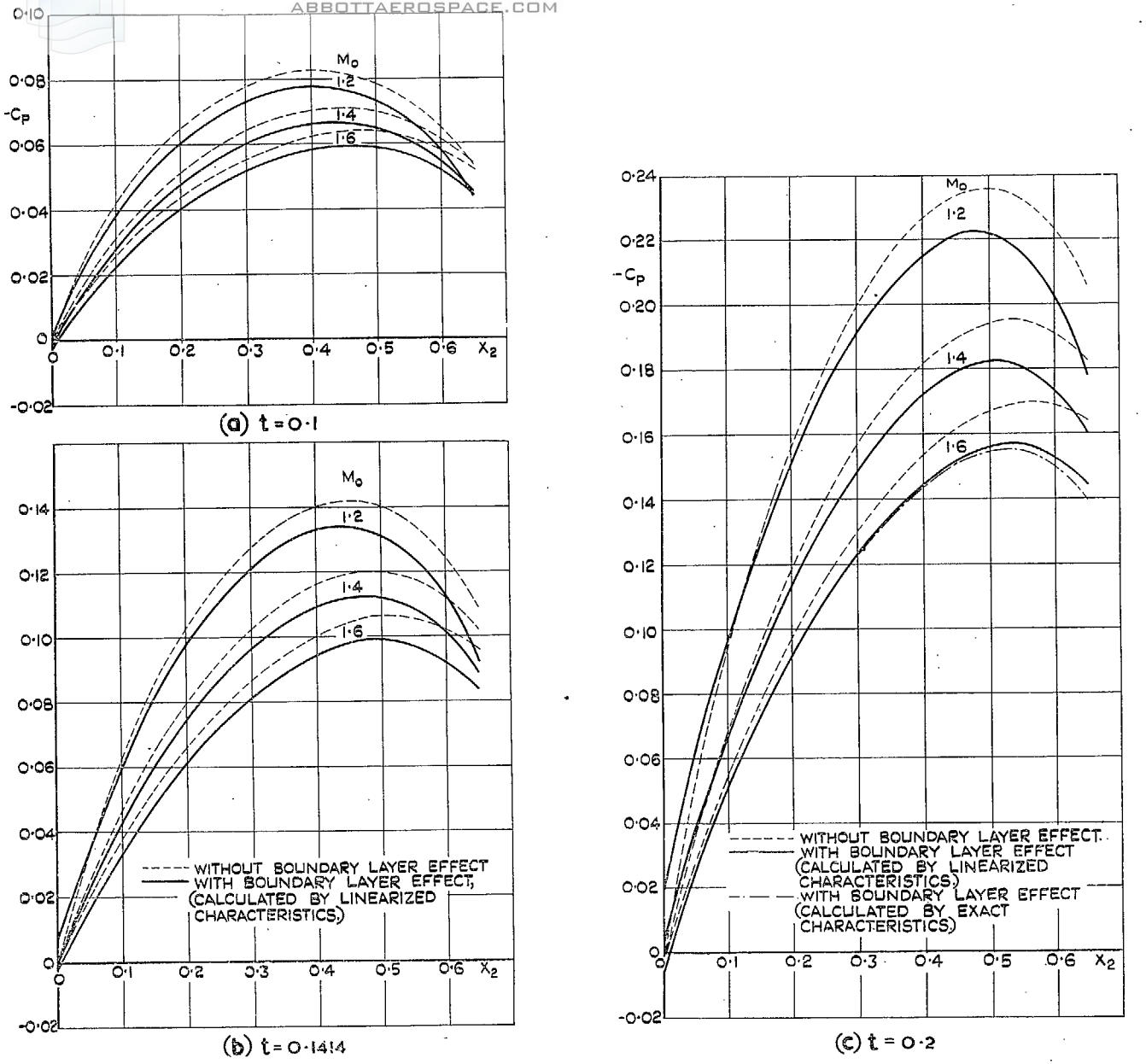

FIGS. 6a, 6b and 6c. Afterbody pressure distributions with and without the effect of boundary layer.

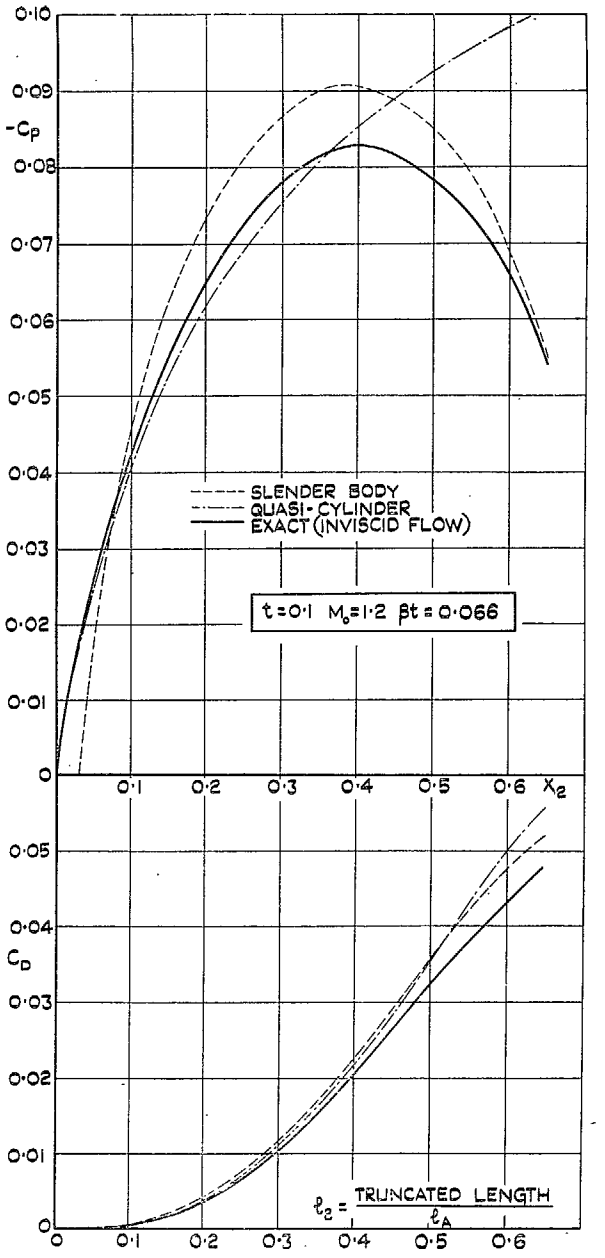

FIG. 7a. Comparison of linearized and exact solutions.

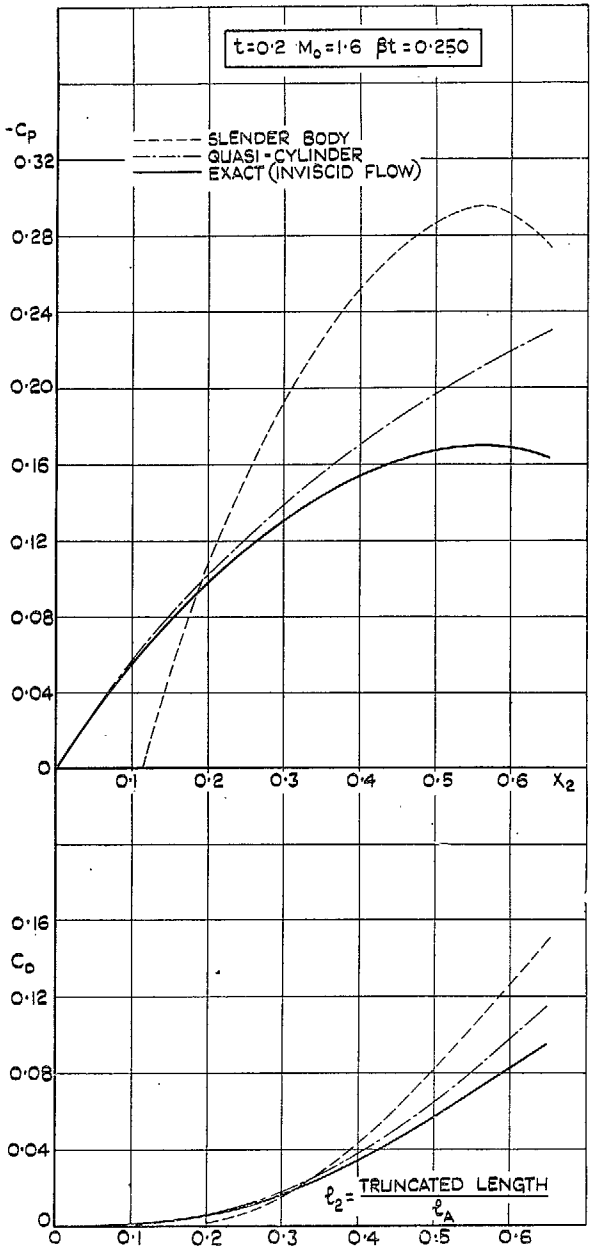

FIG. 7b. Comparison of linearized and exact solutions.

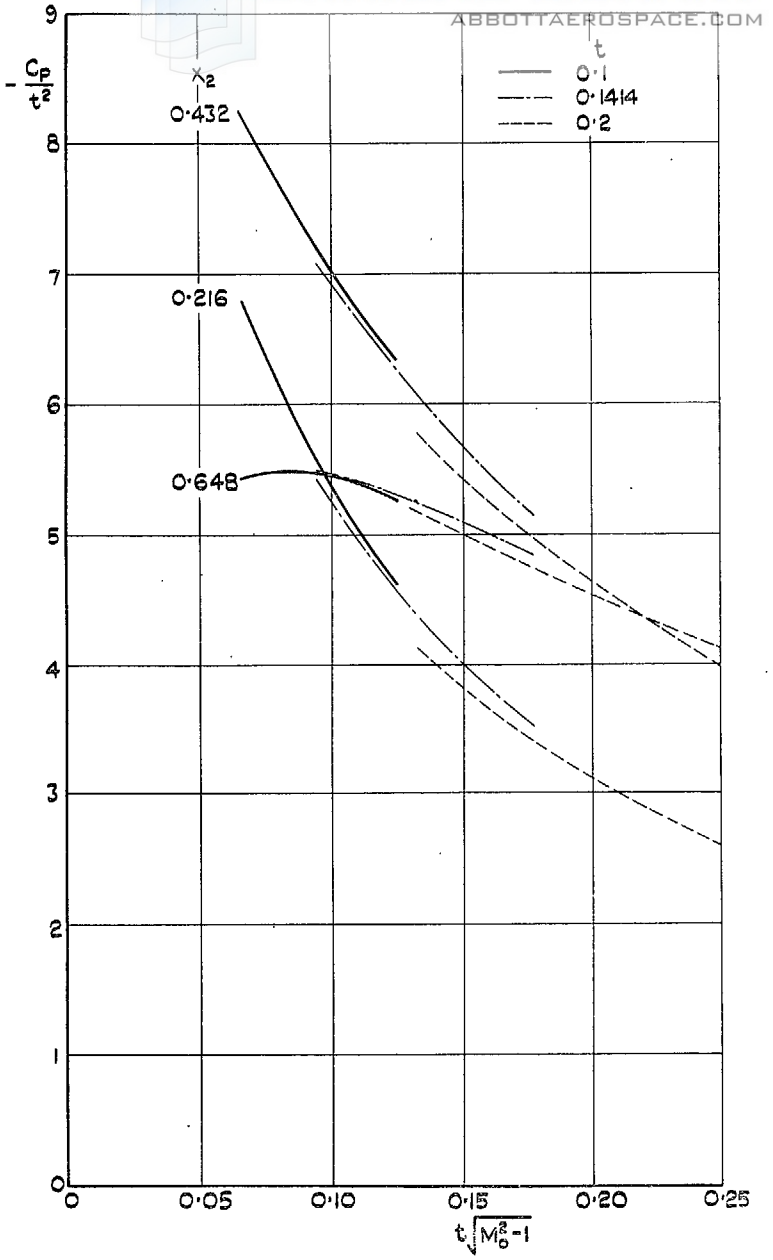

FIG. 8. Afterbody pressure coefficients plotted according to the similarity law.

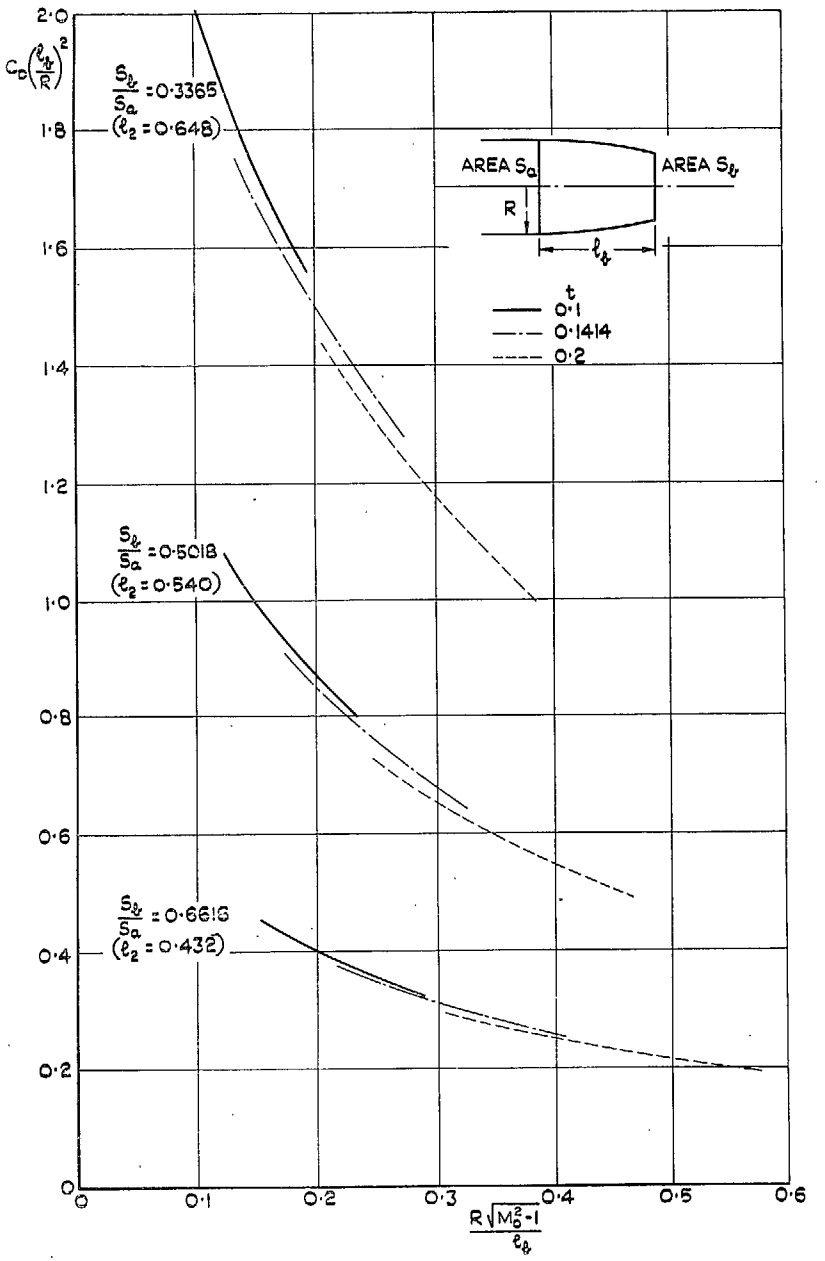

FIG. 9. Afterbody drag coefficients plotted according to the similarity law.

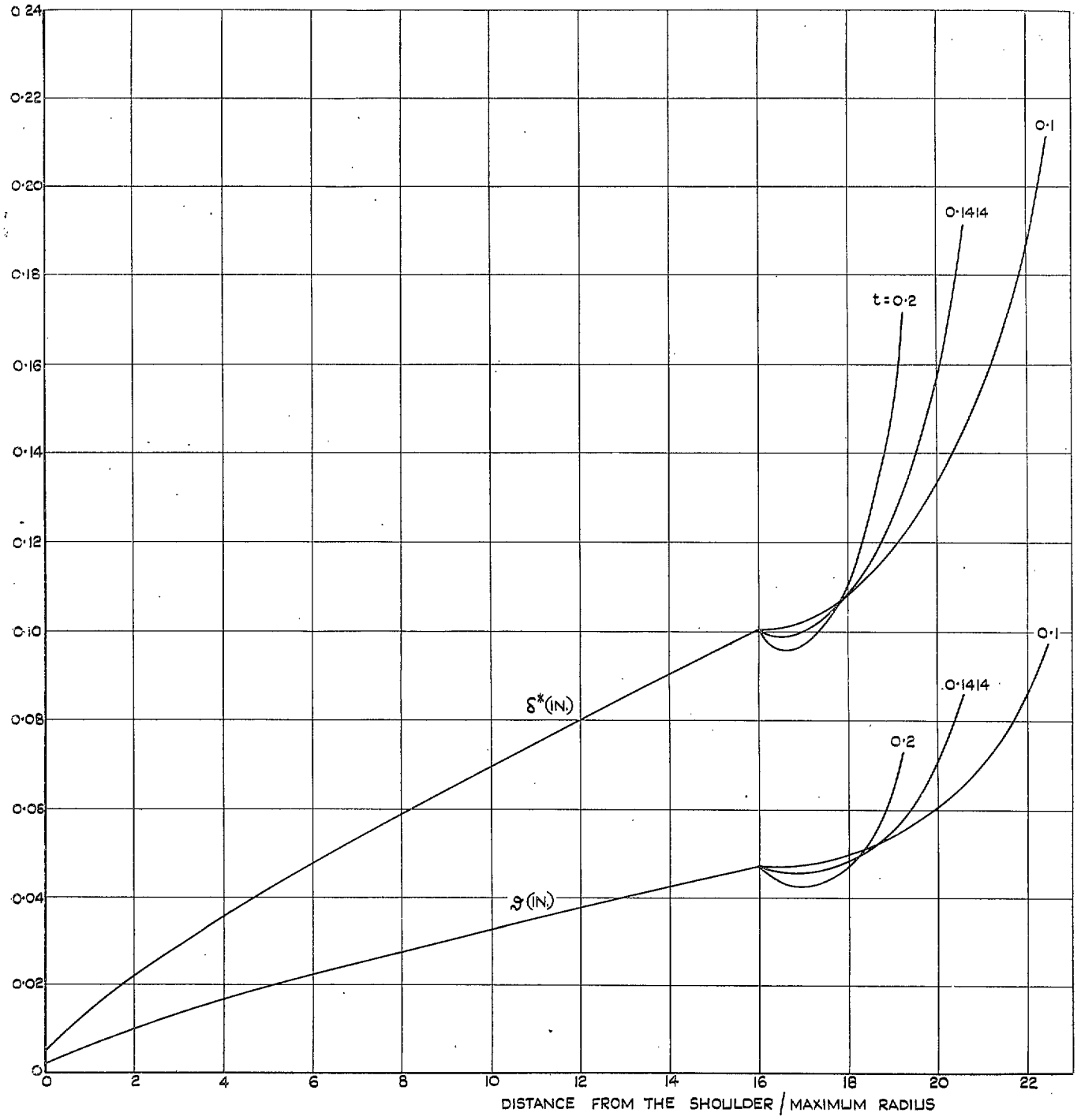

FIG. 10a. Displacement and momentum thicknesses for $M_0 = 1 \cdot 2$.

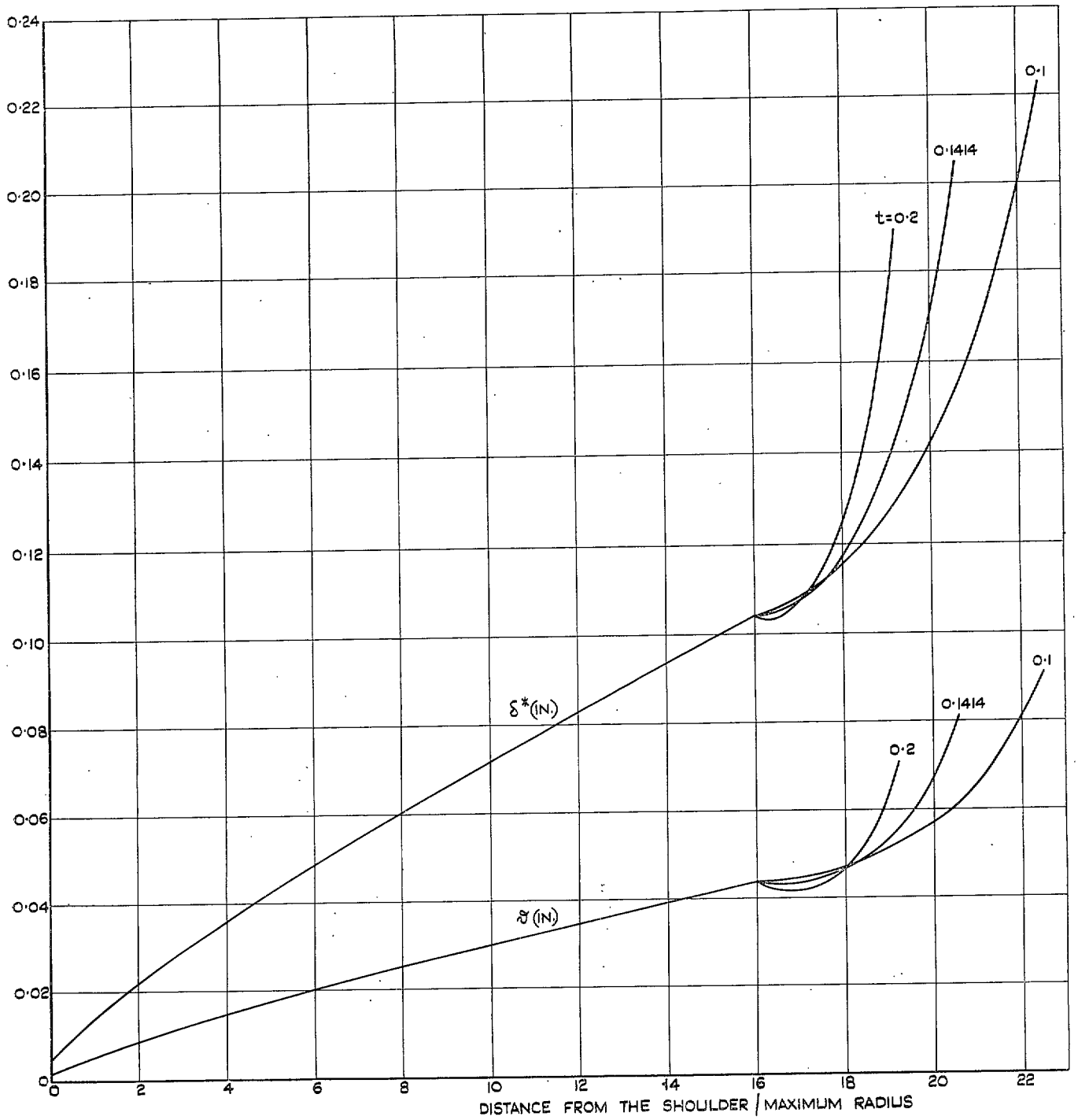

FIG. 10b. Displacement and momentum thicknesses for $M_0 = 1{\cdot}4$.

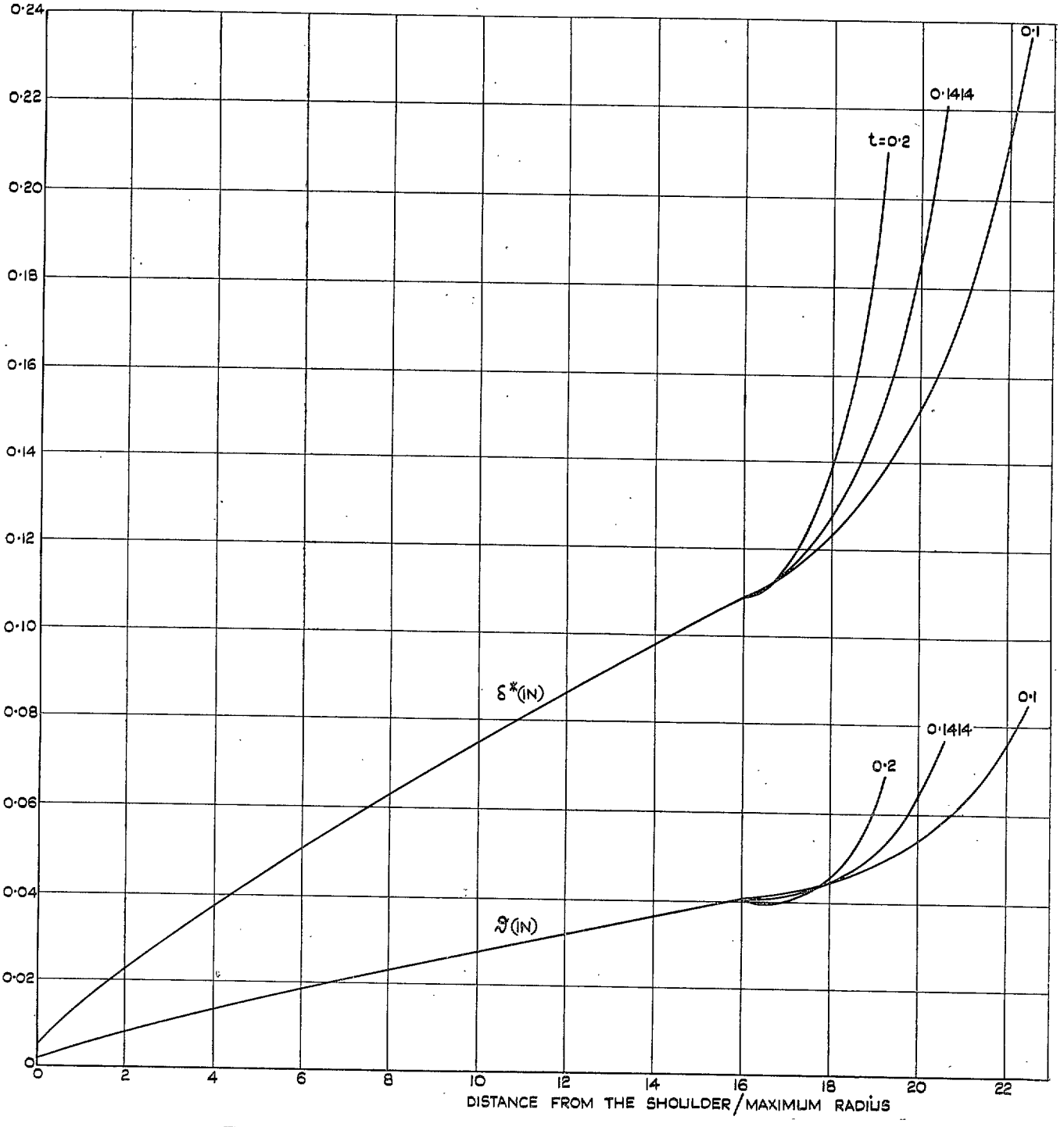

FIG. 10c. Displacement and momentum thicknesses for $M_0 = 1{\cdot}6$.

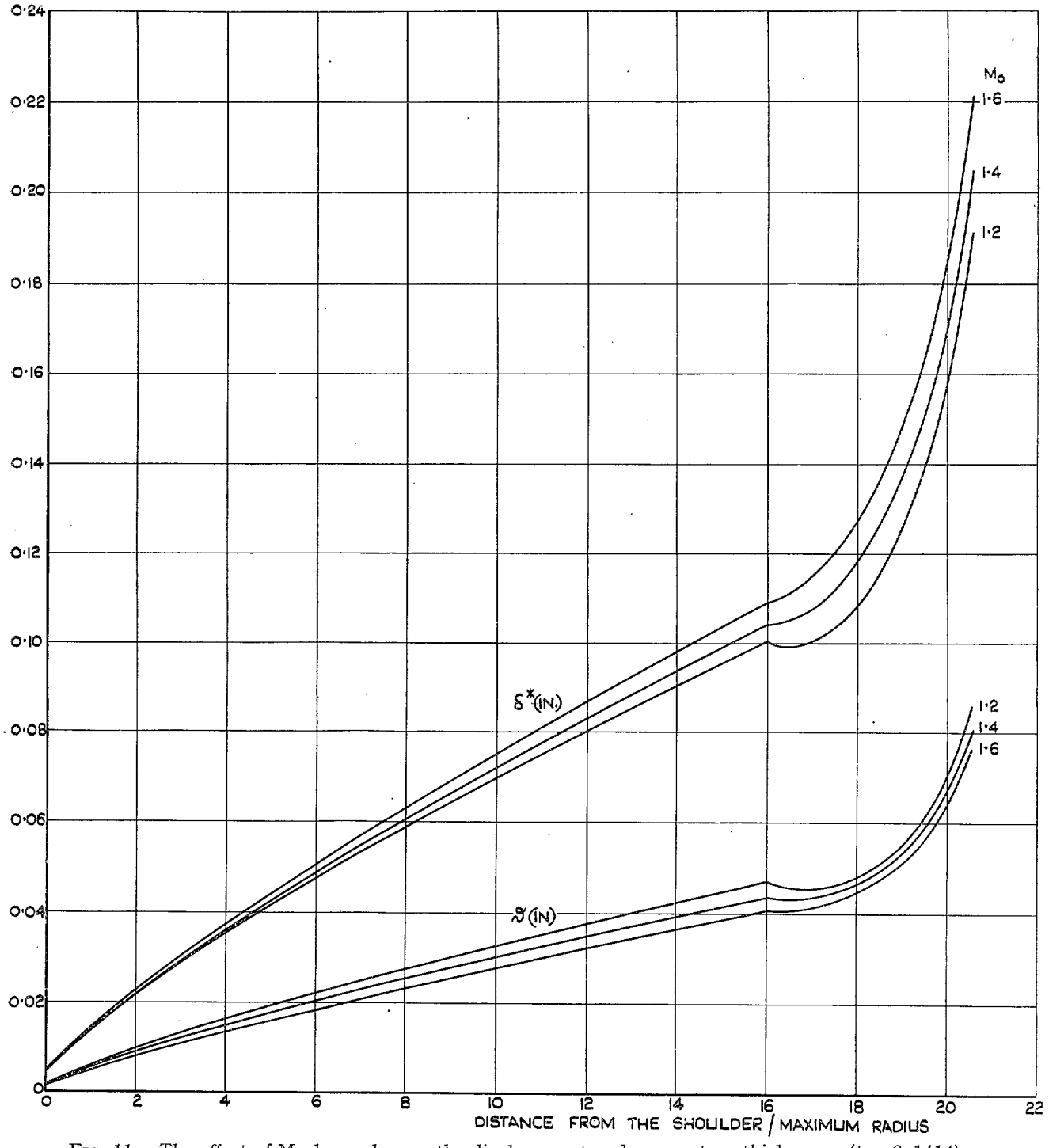

FIG. 11. The effect of Mach number on the displacement and momentum thicknesses ($t = 0{\cdot}1414$).

J4355 Wt.19/8411 K7 11/55 D&Co. 34/263

PRINTED IN GREAT BRITAIN

Publications of the Aeronautical Research Council

ANNUAL TECHNICAL REPORTS OF THE AERONAUTICAL RESEARCH COUNCIL (BOUND VOLUMES)

1939 Vol. I. Aerodynamics General, Performance, Airscrews, Engines. 50*s.* (51*s.* 9*d.*)
Vol. II. Stability and Control, Flutter and Vibration, Instruments, Structures, Seaplanes, etc. 63*s.* (64*s.* 9*d.*)

1940 Aero and Hydrodynamics, Aerofoils, Airscrews, Engines, Flutter, Icing, Stability and Control, Structures, and a miscellaneous section. 50*s.* (51*s.* 9*d.*)

1941 Aero and Hydrodynamics, Aerofoils, Airscrews, Engines, Flutter, Stability and Control, Structures. 63*s.* (64*s.* 9*d.*)

1942 Vol. I. Aero and Hydrodynamics, Aerofoils, Airscrews, Engines. 75*s.* (76*s.* 9*d.*)
Vol. II. Noise, Parachutes, Stability and Control, Structures, Vibration, Wind Tunnels. 47*s.* 6*d.* (49*s.* 3*d.*)

1943 Vol. I. Aerodynamics, Aerofoils, Airscrews. 80*s.* (81*s.* 9*d.*)
Vol. II. Engines, Flutter, Materials, Parachutes, Performance, Stability and Control, Structures. 90*s.* (92*s.* 6*d.*)

1944 Vol. I. Aero and Hydrodynamics, Aerofoils, Aircraft, Airscrews, Controls. 84*s.* (86*s.* 3*d.*)
Vol. II. Flutter and Vibration, Materials, Miscellaneous, Navigation, Parachutes, Performance, Plates and Panels, Stability, Structures, Test Equipment, Wind Tunnels. 84*s.* (86*s.* 3*d.*)

1945 Vol. I. Aero and Hydrodynamics, Aerofoils. 130*s.* (132*s.* 6*d.*)
Vol. II. Aircraft, Airscrews, Controls. 130*s.* (132*s.* 6*d.*)
Vol. III. Flutter and Vibration, Instruments, Miscellaneous, Parachutes, Plates and Panels, Propulsion. 130*s* (132*s.* 3*d.*)
Vol. IV. Stability, Structures, Wind tunnels, Wind Tunnel Technique. 130*s.* (132*s.* 3*d.*)

ANNUAL REPORTS OF THE AERONAUTICAL RESEARCH COUNCIL—

1937 2*s.* (2*s.* 2*d.*) 1938 1*s.* 6*d.* (1*s.* 8*d.*) 1939–48 3*s.* (3*s.* 3*d.*)

INDEX TO ALL REPORTS AND MEMORANDA PUBLISHED IN THE ANNUAL TECHNICAL REPORTS, AND SEPARATELY—

April, 1950 – – – – – R. & M. No. 2600. 2*s.* 6*d.* (2*s.* 8*d.*)

AUTHOR INDEX TO ALL REPORTS AND MEMORANDA OF THE AERONAUTICAL RESEARCH COUNCIL—

1909–January, 1954 – – – R. & M. No. 2570. 15*s.* (15*s.* 6*d.*)

INDEXES TO THE TECHNICAL REPORTS OF THE AERONAUTICAL RESEARCH COUNCIL—

December 1, 1936 — June 30, 1939.	R. & M. No. 1850.	1*s.* 3*d.* (1*s.* 5*d.*)
July 1, 1939 — June 30, 1945. –	R. & M. No. 1950.	1*s.* (1*s.* 2*d.*)
July 1, 1945 — June 30, 1946. –	R. & M. No. 2050.	1*s.* (1*s.* 2*d.*)
July 1, 1946 — December 31, 1946.	R. & M. No. 2150.	1*s.* 3*d.* (1*s.* 5*d.*)
January 1, 1947 — June 30, 1947. –	R. & M. No. 2250.	1*s.* 3*d.* (1*s.* 5*d.*)

PUBLISHED REPORTS AND MEMORANDA OF THE AERONAUTICAL RESEARCH COUNCIL—

Between Nos. 2251–2349. – –	R. & M. No. 2350.	1*s.* 9*d.* (1*s.* 11*d.*)
Between Nos. 2351–2449. – –	R. & M. No. 2450.	2*s.* (2*s.* 2*d.*)
Between Nos. 2451–2549. – –	R. & M. No. 2550.	2*s.* 6*d.* (2*s.* 8*d.*)
Between Nos. 2551–2649. – –	R. & M. No. 2650.	2*s.* 6*d.* (2*s.* 8*d.*)

Prices in brackets include postage

HER MAJESTY'S STATIONERY OFFICE

York House, Kingsway, London W.C.2; 423 Oxford Street, London W.1;
13a Castle Street, Edinburgh 2; 39 King Street, Manchester 2; 2 Edmund Street, Birmingham 3; 109 St. Mary Street, Cardiff; Tower Lane, Bristol 1; 80 Chichester Street, Belfast, *or through any bookseller*

S.O. Code No. 23-2966